Experimental and Numerical Investigation of The Mechanical Behavior of Discontinuous Fiber Composite Structures Under Multi-axial Loading

Minh Nguyen

A thesis
submitted in partial fulfillment of the
requirements for the degree of

Master of Science in Aeronautics & Astronautics

University of Washington

2020

Reading Committee:

Marco Salviato

Jinkyu Yang

Program Authorized to Offer Degree:
William E. Boeing Department of Aeronautics and Astronautics

University of Washington

Abstract

Experimental and Numerical Investigation of The Mechanical Behavior of Discontinuous Fiber Composite Structures Under Multi-axial Loading

Minh Nguyen

Chair of the Supervisory Committee: Marco Salviato

Discontinuous fiber composites (DFCs) are widely used in aerospace and other industries. While being not as strong as traditional unidirectional fiber composites, DFCs are still preferred thanks to its lightweight, ease of manufacturing and aesthetic purposes in application that does not require extreme capabilities. However, DFCs have the potential to be used for complex and critical components like joints and braces, of which difficult to use traditional continuous fiber composites. Such components are naturally subjected to mixed mode loading conditions. The focus of this thesis is to explore the response of DFCs under multi-axial loading conditions to have a better understanding how this material behave. The multi-axial loading was applied using the Arcan rig adapted from Yao *et al.* [39, 40]. A modification of the Arcan rig system was made to ensure the correct bi-axial failure for DFC coupons. Experimental results showed that the DFC test specimens exhibit similar stiffness and strength to quasi-isotropic layups in pure tension and pure shear, while the energy release per volume amount is lower than the traditional layup. Stochastic finite element model of DFCs adapted from Ko *et al.* [41, 42] using random platelet generation algorithm combined with Hashin failure criteria was developed to capture the multi-axial behaviors of DFCs. The model managed to capture the strength of DFCs accurately but showed limited accuracy in terms of the non-linear behavior due to shear load. The experimental and numerical analysis of DFCs under the multi-axial loading demonstrated unique structural behaviors of DFCs. This study provides a valuable set of data for engineers and designers who wish to calibrate their model under the multi-axial loading conditions.

TABLE OF CONTENTS

Page

LIST OF FIGURES

LIST OF TABLES

GLOSSARY

CFRPS: Carbon Fiber Reinforced Plastics

DFCS: Discontinuous Fiber Composites

DIC: Digital Image Correlation

QI: Quasi-isotropic

UD: Uni-directional

ACKNOWLEDGMENTS

The author wishes to thank Professor Marco Salviato and Professor Jinkyu Yang's guiding for academic opportunities for growth and learning. The author also thanks Seunghyun Ko for three-year long of mentorship. The author also wish to express gratitude to Bill Kuykendall for his experimental facility supports and MAMS team members for their helps, and finally family and friends for their inspiration.

Chapter 1

INTRODUCTION

In recent years, carbon fiber reinforced plastics (CFRPs) have become a very popular material in many industries such as automotive, aerospace, tools, sports, etc.. One of the main selling point of this material is its high strength-to-weight ratio [2,4,5,29]. In general, carbon fiber is five times stronger than steel, and yet lighter than aluminium [1, 2, 4, 12]. This makes CFRPs ideal materials for any application in which weight plays major roles, like aerospace and automobiles [5, 39, 48]. For different applications, CFRPs can exist in different forms. Beside the traditional unidirectional (UD) or woven fiber, it can be made with short carbon fibers or milled carbon powders [2,4,5]. Beside those alternatives, another unique variation is discontinuous fiber composites (DFCs), which is the focus of this thesis. Due to the size of DFCs' building blocks, it can be perceived as the medium between short fiber and traditional UD (Fig. 1.1) [2, 10, 41, 42].

1.1 Discontinuous Fiber Composites (DFCs)

DFCs are CFRPs using randomly oriented fibers [2,10,37]. The smallest unit that builds up DFCs are called platelets, which exist in mesoscale, with size can vary from a few millimeters to a hundred millimeters [37, 48]. Due to that, DFCs' property is inherently different from conventional CFRPs like short fibers or UD fibers. The stiffness is comparable to quasi-isotropic laminate [32, 35, 48]. However, when comparing strength-wise for a completely randomly oriented DFC, it is definitely weaker than UD [29, 32, 37]. In CFRPs, carbon fibers carry most of the load. With the fibers disconnected, DFCs cannot carry as much load as UD. However, it has other unique properties that make it stands out.

Study has shown that with fibers randomly oriented, DFCs can achieve in quasi-isotropy [26, 32, 37, 42], which means isotropic behavior in-plane, or similar to metal. Therefore, it would behave in the same manner when subjected to loading in different angles or ori-

(a) Bicycle crank set

(b) Lamborghini engine cover

Figure 1.1: Example of commercial DFC

entations. This simplifies the engineering processes like material modeling and structural design. On the other hand, UD material is only strong specifically in the fiber direction. To acquire balance performance in all directions like DFCs, the composite layup requires UD plies to be angled in multiple directions of $0°/\pm45°/90°$. The laminate property then can be considered quasi-isotropic. This gives DFCs advantage over UD in manufacturing complexity and labor.

Furthermore, with the existence of notches or cracks, traditional laminates usually show decrease in strength. DFCs, on the other hand, exhibits notch insensitivity [11, 15, 23, 35–37]. This behavior has been shown from studies to be dependent on structure size, structure thickness and platelet size [41, 42]. Tang *et al.* also showed that DFCs show strong notch insensitivity, and even through cyclic loading and fatigue [15]. This is a very desirable property for CFRPs. Current manufacturing processes often times require drilling holes for bolting, or riveting two pieces of composite together [54]. During those manufacturing processes and component's lifetime, notches, cracks formed would introduce stress concentration, this would eventually lead to early failure for brittle materials like CFRPs. Therefore, notch insensitivity trait of DFCs is highly sought after in modern applications of composites.

Furthermore, DFCs have scaling effect that can affect the notch sensitivity, as well as

general material behaviors, as size varies. Many studies showed that DFC is strongly under influence of size effect law proposed by Bažant *et al.* [9]. Ko *et al.* showed that the behaviors may shift from typical brittleness of CFRPs [24,25,27,31,44–46] to more of pseudo-ductility as structural size reduces, or increase in platelet size [42]. In addition, the strength also increases according to the thickness, and plateau after certain capacity [41]. In short, DFCs are unique materials whose properties can be optimized from platelet size, structure size and structure thickness. Having more controllable design parameters makes DFCs a versatile option.

1.2 Industrial benefits

From the industrial point of view, DFCs are a very attractive option, due to potential of cost/waste reduction, manufacturing complex components and recyclability [21, 34]. Traditional UD laminates are often made using layup methods. Thus, it can only make 2D structures like plates, tubes, and some other simple 3D shapes like mechanical booms or wheel drums. Therefore, manufacturing with UD laminates can be limited due to componen'st structural complexity. On the other hand, those limitations do not apply to DFCs, due to the fact that DFCs are made from smaller platelets, which can flow and form 3D shapes [10,34–37] (Fig. 1.2). Furthermore, along with compression molding, no layup would be needed, and the time required to cure can be as short as two minutes [1,10], while typical UD layup may requires days to complete, and hours for curing [12]. This give DFCs huge advantages in mass production, manufacturing complex component and reducing labor cost.

Regarding recyclability, this comes from the fact that DFCs can be made from uncured scrap UD [21]. Fabrication of UD laminates usually produces of lot of raw waste [2]. As the usage of CFRPs increases, so would the issue of waste reduction from manufacturing. As a solution, uncured scrap materials can be either chopped to make DFCs. Depending on the quality of the waste, other ways would be going through either chemical or pyrolysis process to extract carbon fibers and remake them into DFCs or short fibers composites [2]. Along with labor cost, using recycled DFCs would be cheaper than using UD material [32].

Figure 1.2: DFCs prototype of F-1 engine's impeller

1.3 Advanced uses of DFCs

While there are many advantages in using DFCs as substitutes for UD, their potential can be more than just as a simple material. As mentioned above, DFCs is made from randomized small platelets. Therefore, the material's properties can also be tailored for specific needs. Longana *et al.* have done some studies on aligned DFCs. By adding aligned DFCs along with UD laminates, the result laminate showed pseudo-ductile response [30]. In another study, DFCs with platelets made from thin tow showed increase in strength compare to typical DFCs, it was found to be even stronger than aerospace grade laminates [29]. In other fields like electrical, carbon fiber is also known for its high conductivity [2, 4, 5]. In radio transmission, Arter *et al.* showed that DFCs have high homogeneity compare to typical CFRPs. Along with weight advantage, this makes DFCs great materials for antennas. Furthermore, under certain wavelengths and bandwidths, DFCs can perform just like any other isotropic material [13].

1.4 Current problems and focuses

DFCs, in many ways, are versatile materials. It has many unique properties that are highly sought after in conventional CFRPs. There have been many studies about damage initiation and molding quality [23, 49]. Many numerical models have been proposed for studying DFCs. Feraboli *et al.* created DFCs' model by discretizing material properties in

each element partition, which successfully capture non-uniform strain field [37]. Selezneva *et al.* created stochastic 2D model that can determine the material's strength and effect of platelet size base on the principle of weakest link [32, 48]. Machine learning models are starting to be used as well. Pimenta *et al.* implemented Bayesian optimization routine to improve efficiency of virtual testing framework for aligned discontinuous fiber [21]. Thanks to the past researches, DFCs are now used for secondary structures and aesthetic purposes like window frames and automobile's interior and body parts [7, 37].

However, there are many aspects of DFCs still being studied. Currently, the effect of out-of-plane and mode I fracture mechanism is still being researched; another would be new joining methods for DFCs in manufacturing [54]. Best of author's knowledge, the shear property of DFCs is still not yet fully discovered. Thus, the usage of DFCs for critical components or primary structures is still very limited. If DFCs' capability were push to the limit, this material would be more suited for fabricating intricate components like joints and hinges. However, due to their 3D complex geometries, they are prone to be subjected to multiple loading conditions at the same time [33]. Unfortunately, there are also no studies about DFCs in mixed-mode loading condition, whether it's experimental or numerical analysis. To be able to fully utilize DFCs for industrial uses, it is necessary to have a complete working model of this material in those conditions. Therefore, the goal of this study is to get a better understanding of this material under multi-axial loading experimentally, as well as establishing Finite Element model that can capture accurately the response of the structures for future applications.

Chapter 2

MANUFACTURING DFCS SPECIMENS

2.1 Regarding the option for commercial DFCs

Currently, there are suppliers that produce commercial DFCs. A well-known production line is HexMC® made by *Hexcel Corporation* [10], which has been used for manufacturing window frames on Boeing 787. There are other manufacturers like Toray, Teijin, Quantum, etc. While manufacturing test specimens can be done using commercially available DFCs. There were many reasons why in-house manufacturing is preferred. Such reasons are described as follow.

First, different manufacturers would produce different platelets size and shapes. Therefore, the quality of DFCs obtained would differ by using different sources. Furthermore, for researching purposes, there would be many research topics and focuses that platelet's geometry needs to be fully in controlled. Ko *et al.* performed some experiment on the effect of platelet size in predicting DFCs' strength and toughness [42]. Selezneva *et al.* also conducted studies on multiple platelet lengths [32].

Second, it is hard to control the thickness of laminates with commercial DFCs. When purchased, DFCs usually store in a similar fashion to prepreg. The prepreg platelets are randomized, pressed firmly together as a sheet and rolled up between non-stick paper layers. In this form, raw DFCs would come with certain thicknesses. As mentioned above, DFCs are usually manufactured using compression molding without the need of layup process. It means that for different components, raw DFCs will have to be with different thicknesses to achieve the component's final dimensions.

Furthermore, DFCs is very sensitive with changes in thickness. Its strength would increase proportional to the thickness, and plateau after certain limit [41]. And so, it is very important to be able to adjust the thickness as needed.

Finally, it is necessary to know DFC platelet's material properties. One of the purposes

of DFCs is to reuse scrap materials from UD layups. Therefore, the scrap materials, which is the source material for DFCs, may come from different origins. This would be a challenge to determine the material properties of the platelets, either from identifying the sources, or through homogenization.

To sum it up, even though it is very convenient to use commercially available DFCs, it is hard to control many specifications and parameters of the final product, like thickness, platelet's geometry and material properties. Thus, DFCs specimens would have to be manufactured from the lab from scratch, using known UD for full control in both quality and consistency.

2.2 In-house manufacturing process

Many of the specifications were adopted from Ko *et al.* [41, 42] and HexMC® [10]. The purpose is to manufacture DFC specimens with known material and geometry specifications. The raw material used for manufacturing is prepreg T700G-12K series from Toray. The platelet dimension was chosen to be 50×8 mm to match with commercial platelet size of HexMC®. When using prepreg UD to make small platelets for DFCs, there are several issues to be addressed. The process has to be capable of manufacturing a large amount of platelets ($\sim$ hundreds to thousands) with the correct dimensions. It also has to be able to remove all of the backing papers from those platelets. In addition, it must achieve consistency in randomization. Finally, for making a large amount of samples, time efficiency is necessary. The following procedures of making DFCs met all of the requirements and was used in this research.

2.2.1 Making raw DFC plies

Logistically speaking, it would be impossible to remove backing paper from individual platelet. The process would not only be time consuming, but also likely to damage and deform the platelets. Thus, the paper has to be removed before cutting the prepreg to smaller pieces. Having said that, the paper should not be removed at the beginning to avoid contamination from the working surfaces.

First, the prepreg UD is cut using CNC fabric cutter with a square-cornered zig-zag pattern running along the fiber direction. The result of the cut can describe as a pair of comb-like pieces intertwined with each other. The width of each "comb teeth" is 8 mm, and the length is roughly 1 meter, with the total width of the comb is about 200 mm. The total length and width of comb can be adjusted for the ease of handling, thus there are no strict measurements to follow (Fig.2.1a). After the cut, the pair is separated into individual combs.

During the handling of the combs from then on, the strands may stick to each other. To prevent that, a strip of tape is applied at the free tip on the fiber surface. The comb is then laid fiber face-down on a layer silicone paper, which is also commercially called parchment, or baking paper (Fig.2.1b). This make a clean and non-stick working surface. Next, the backing paper is peeled, then a second silicone paper is applied on top, making a sandwiched comb. Beside being a working surface, silicone paper also prevents the peeled combs from sticking to itself and others. This is important to assure good platelet quality for randomization.

Finally, the sandwiched comb is moved back to the CNC cutter. Figure 2.1c top silicone paper can be removed for later use. The cutter then performs multiple straight cuts across the comb teeth with 50 mm in spacing in-between along the whole length. The result are 50×8 mm platelets laid on a piece of non-stick paper and ready to for the next step (Fig. 2.1d).

To randomize, the platelets are handled using the silicone paper and then shaken to a container. The randomization happened when the platelets are shaken and free falling into the container, which results in random arrangements (Fig. 2.1e). Naturally, the distribution of platelets would be highest at the center and very little at the edges. However, the goal is to make good randomization but with consistent thickness overall. Therefore, the platelets are purposely shaken toward the edges instead, as well as regions of detectable difference in thickness.

Through trials and errors, it is found that thickness and randomization is better controlled when making 100 gram ply individually. After making separated thin plies of DFCs, they can be stacked together to form the complete layup. During the randomization process,

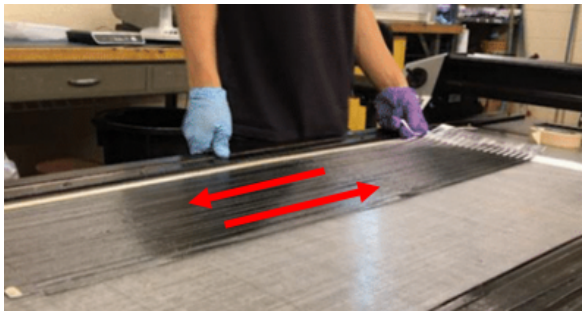

(a) Zig-zag pattern cut for making combs. Each 'comb tooth' is 8 mm wide.

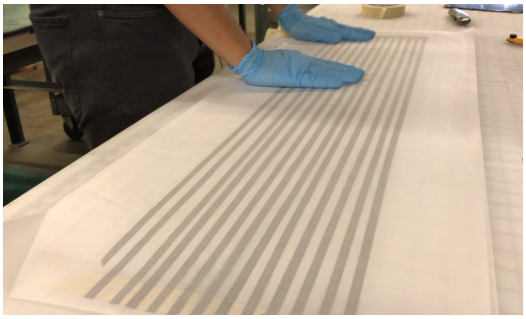

(b) Silicone paper prevents sticking when removing paperback and transporting.

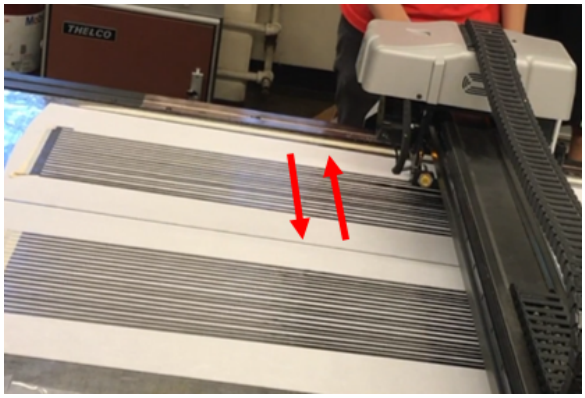

(c) Cross cut of the comb, distance between each cut is 50 mm.

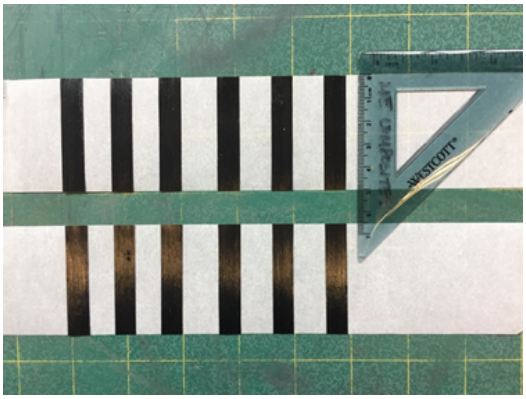

(d) Platelet produced with the dimensions 50×8 mm as desired

(e) Platelets are randomized by shaken into container.

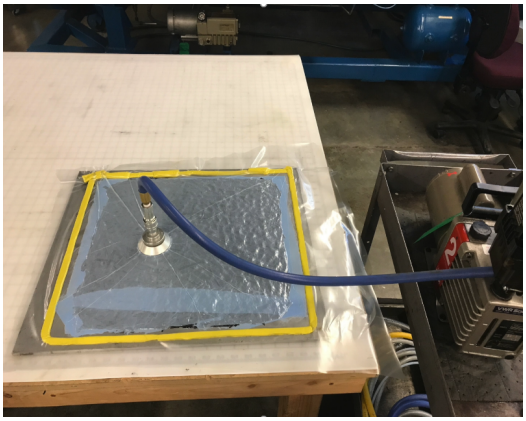

(f) Debulk DFCs at 1 atm for 30 minutes to reduce air gaps

Figure 2.1: In-house platelet manufacturing process

air pockets and gaps may exist and reduce DFCs' strength. Therefore, the raw DFCs have to be debulked for every additional 400 grams, or four stacks. The debulk process runs at 1 atm for 30 minutes (Fig. 2.1f). Unlike traditional layup, the thickness of DFCs cannot be determined by layers but from weight instead. From past trials, it was determined that to make a 15×15 in and 3.3 mm thick panel of DFC, the panel requires 768 grams of platelets. From other researches, DFCs' properties plateau after reaching 3mm in thickness [41]. And so, the panel's thickness was chosen with purpose to reduce uncertain factors between DFC specimens.

2.2.2 Curing DFCs and Preparing Specimens

After obtaining raw DFCs, the next step is to cure. The ply is placed inside a flat aluminium compression mold 16×16 in, then put inside heated-platen press. The machine in use is Wabash G50H-24 50 ton. The curing process is followed from Toray's instruction [12]. The recipe has 1 hour ramping from 100°F to 270°F, 2 hours soaking at 270°F, and finally 45 minutes cooling from 270°F to 80°F. A pressure of 88 psi is applied during the whole curing process. Usually after curing, there are discolored epoxy, dry spots and dry fibers along the edges. Those would be removed by trimming away 1 inch of the edges. The final product is a edge-trimmed DFC panel.

To create sharp notches at the gauge section, watterjetting has to be used (Fig. 2.2b). The specimen design will be explained in the following section about testing apparatus. After waterjetting, the specimens are tabbed using glass fiber panels. This prevents failure at the clamping border or inside the clamp due to clamping pressure, and also to maintain consistent stress flow. For bonding, Locktite E-60HP is used. Before applying adhesive, the contact surfaces of the specimens and tabs are all to be sanded. Sanding helps roughen the gloss surfaces and improve bonding quality of epoxy. The final step of preparation is paint speckle pattern for Digital Image Correlation (DIC), which will be used to collect strain information.

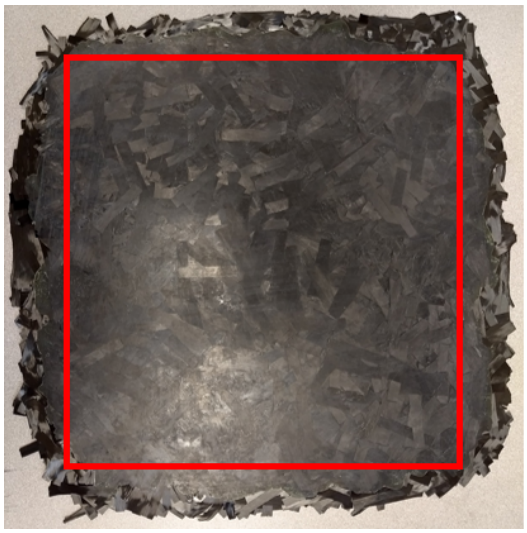

(a) Cured DFCs have discolored epoxy and dry spots, to be trimmed 1-2 inches from edges

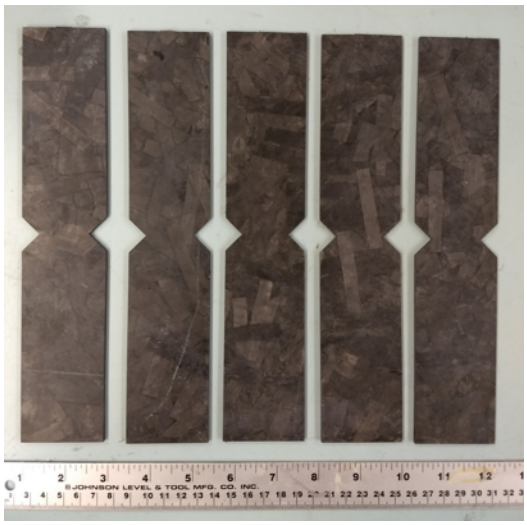

(b) Waterjetted specimens with notch design.

(c) Sanded, cleaned specimens and tab tiles before bonding

(d) Speckle painted specimen for DIC analysis

Figure 2.2: Cutting and tabbing specimens

Chapter 3

TESTING APPARATUS AND SPECIMEN DESIGN

3.1 Choosing the suitable test system

There are mulitple methods to apply multi-axial loading condition. The typical tests are cylindrical torsion load, cruciform biaxial loading, iosipescu test and also Arcan fixture test. Each method provides different load mixture, and from them the most suitable type is chosen as the main testing method.

Cylindrical torsion test creates shear and tensile load. However it can only be used for tubular specimens. Cruciform biaxial test requires making complex cross-shape specimen (Fig. 3.1a) with intricate curved corners to prevent stress concentration [33]. Using four different actuators, the system can perform tensile/compression loads in both longitudinal and transverse direction, and pure shear. The specimen's shape is not very convenient for manufacturing time and efficiency. Furthermore, biaxial test require specific load frames, which is not available.

Iosipescu is a simple method to perform pure shear test following ASTM standard [20] (Fig. 3.1b). With some modification, some are called double railed test [16]. It is known for providing good shearing condition. However, with commonly used fixtures, it is limited to small specimens only. It also can only provide pure shear load, not mixed loads.

Arcan fixture (Fig. 3.1c) was originally used in 1980 was a method to measure shear modulus of composites [6]. The test required only a simple tensile load frame and a circular plate fixture to orient specimen in side-way direction with respect to loading direction to achieve shear load. However, by adjusting the angle between the specimen and loading direction with rotation the fixture, mix load of tension and shear can be done.

Considering the Arcan fixture test only requires simple load frame and the fixture, which is also acquired, it is the most suitable testing methods available.

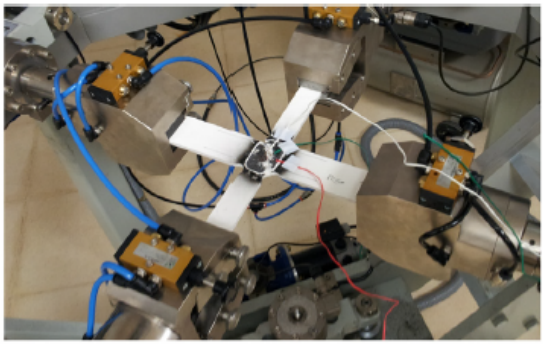

(a) Biaxial test with cruciform specimen [33]

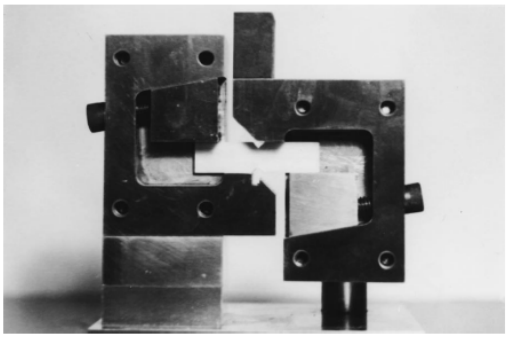

(b) Iosipescu test for pure shear [20]

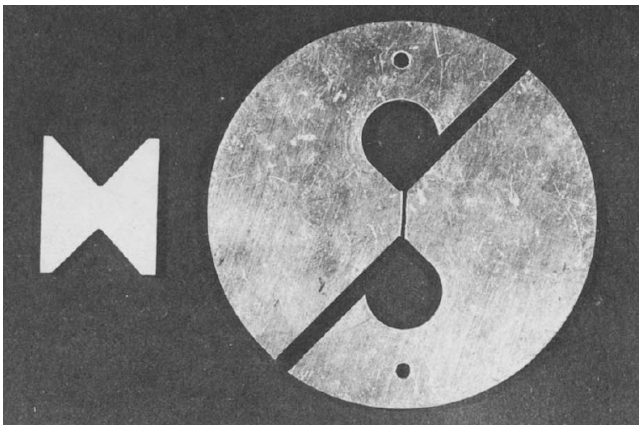

(c) Original Arcan fixture for testing shear modulus [6]

Figure 3.1: Fixtures for bixaxial and shear load

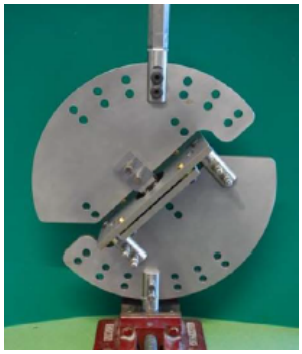

(a) Mounting system for bolted specimen [14]

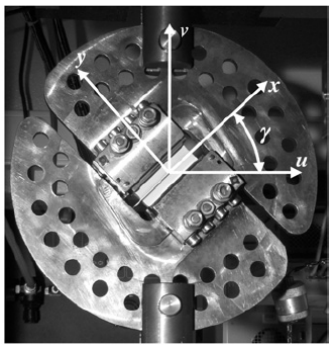

(b) Multi-axial test for out-of-plane properties [22]

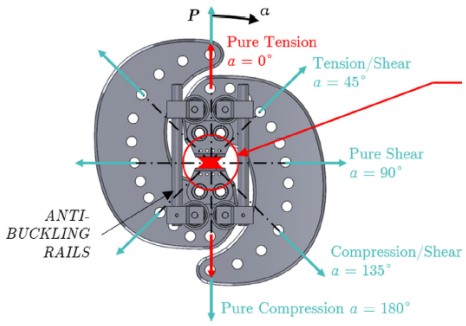

(c) Anti-buckling rail for compression loading mixture [47]

Figure 3.2: Modified Arcan fixtures for different problems

3.2 Modification to Arcan Fixture Testing System

Unlike the original design, the modern fixture contains a lot of pin slots for a wide range of loading angles 3.2. There are a lot of creative uses of the fixture. Cognard *et al.* used Arcan fixture to test out-of-plane behaviors of composite, confirming the ability of the fixture (Fig. 3.2b) [22]. Later on, they determined 3D failure envelope for composite using data acquired from the same loading configuration. The specimen used had a wide contact surface for bonding and reducing edge effect [28]. In other cases, Pearce *et al.* used Arcan fixture to replicate the mixed mode loading on bolts holding composite panels (Fig. 3.2a) [14]. Different load mixtures would result in different type of failures, like bolt pull-through or delamination. Finally, there was a study of composite of mixed mode loading that involved compression. Guiding rails were installed on the fixture for buckling behavior (Fig. 3.2c) [47]. In general, there are several modified versions of the Arcan fixture. However, one thing in common is that the multi-axiality of the loading relies on the rotated angle of the fixture, while keeping the specimen in the very center. As long as the mentioned principle is maintained, other modifications can be done according to the specific purposes of research.

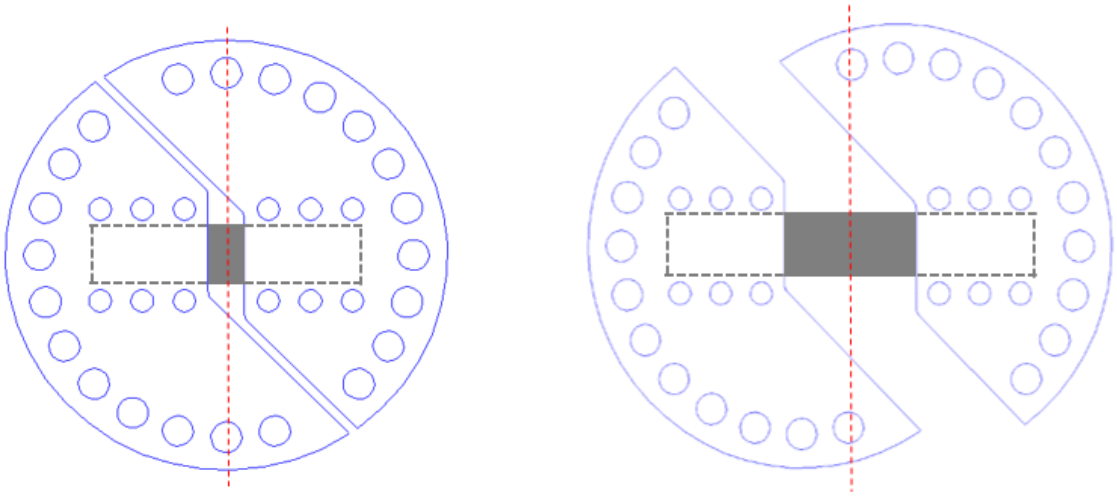

(a) Arcan fixture was designed for 20 mm gauge length (gray). Pin slots aligned with red axis are used for shear test.

(b) By aligning different pin slots for shear test, longer specimen with 90 mm gauge length can be used

Figure 3.3: Expand Arcan fixture to test larger specimen

3.2.1 Redetermine Arcan Angles for Large Size Specimen

The Arcan fixture available from the facility was designed to be used for specimens with gauge area of 50mm in width and 20mm in gauge length [39, 40]. Under those specific dimensions, the fixture would be able to orient specimen in determined angles of 0° / 15° / 30° / 45° / 60° / 90° and so forth, with 15° increment. However, manufactured DFCs' smallest identifiable unit is a 50×8mm platelet. Statistically speaking, it is very necessary to be able to capture the whole platelet in the gauge area. The test has to be able to capture the full response of the smallest representation of the material, or a single platelet in DFCs. For that to happen, the gauge area has to be large enough to encapsulate whole platelets. Therefore, the default specimen dimensions for the Arcan fixture is not suitable for DFCs. Thus, there is neeed for redesigning the specimen's geometry.

In theory, Arcan fixture can be used nevertheless of the specimen's length. However, in multi-axial studies, it is crucial to capture the behaviors at critical angles like pure shear

(90°) and 45°. For pure shear, it means that there has to be a pair of pins that align with the center of the specimen at 90° setting. Incidentally, the fixture has a pin pair that was designed for 105° loading by default. As a solution, by using the 105° pin as 90° pin, longer specimen can be tested and observed in pure shear condition (Fig. 3.3).

After calculating the dimensions, instead of 20 mm, the specimen's gauge length would have to be 90mm. And from modified length, the testing angles available would be as in the Table. 3.1. The bold angles are the ones that do not differ greatly and will be use for the experiment. This modification of the fixture's usage does not involved with specimen's width. And so, the width is decided to be 50 mm, which is the maximum size allowed with this fixture. Having a larger specimen would help increasing the likelihood of capturing whole platelet in the specimen.

Pin	Default angle (deg)	Redetermined angle (deg)
1	-45	-36.51
2	-30	-24.17
3	-15	-12.04
4	**0**	**0**
5	15	12.04
6	**30**	24.17
7	**45**	**36.51**
8	**60**	**49.18**
9	75	**62.31**
10	**90**	76.07
11	105	**90**

Table 3.1: Recalculate loading angles

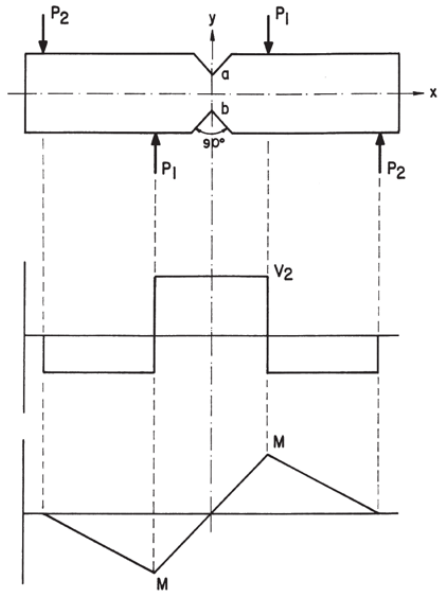

Figure 3.4: Load distribution of an Iosipescu specimen [20]

3.2.2 Determine Specimen's Geometry for Pure Shear

It was mentioned above that the specimen's design would have to include deep notches (Fig. 2.2b). The reason for that is to guarantee pure shear failure during pure shear loading condition. When subjected to pure shear, the Arcan fixture behave similarly to the iosipescu test. Fig.3.4 describes the load distribution during the shear test during iosipescu test [20]. The asymmetrical designs of the iosipescu and Arcan fixture allow symmetric loading from the very center of the specimen towards both ends. However, it can be easily observed that the loading condition is very similar to shear load on single cantilever beam. Therefore, beside shear load, there are also bending moment created due to shear. Naturally, material would fail where stress reach critical value the earliest. For a typical uniform specimen with no defects, usually that region would be where shear load and bending moment at their highest, the clamping border of the gauge area.

One common approach to this problem is to reduce the stress from bending moment. It has been noticed that many experiments conducted were with specimen with minimal length [6,28,47], from a few millimeters to only a few ply thick. When the specimen's length

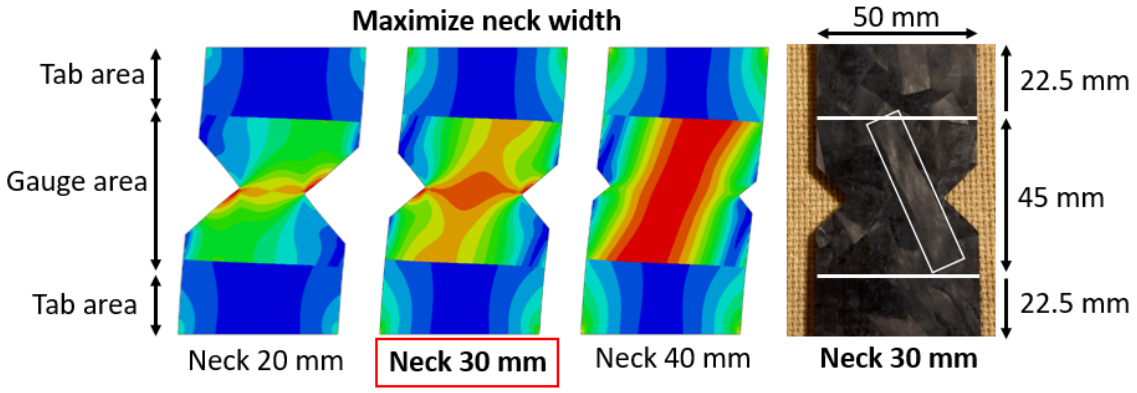

Figure 3.5: Stress field shows that notch 10 mm deep combined with extra tab areas guarantee highest stress concentration at the middle and notch tip, which leads to failure.

ratio is very small, the bending moment can be considered negligible. Having said that, the specimen for this study is very large, and the effect of bending moment increase more so.

For a long specimen is to fail due to pure shear, it has to be where there is no bending moment, which is the very center. And so, the middle is designed to be the weakest region. Hence, "defects" are typically introduced to allow stronger stress concentration at the middle to ensure failure at designated location. Typically notches, cracks or circular holes are introduced, since they effectively represent common structural defects in real parts [17]. Since the objective of this study does not involved with defects, cracks and open holes was not chosen as a method to weaken the specimen, but notching instead. Although notches are also considered to be defects, that would be subjective depending on its size compared to the structure size. If notches are large enough, it would not be considered as a defect but a structural property. On the other hand, the depth of the notches should be limited to maximize the gauge area at the center. In general, the notch is designed to have an angle of 90◦ [20]. However, despite the notch's depth reaching 40% of the cross section area, the failure would still happen at the clamping border. With a gauge length of 90mm, the effect of bending moment is not feasible to overcome be having notches alone. Therefore, another solution proposed is to increase the thickness of the gauge region near the border by lengthening the fiber glass tabs out from the clamp. With the thickness increase, the

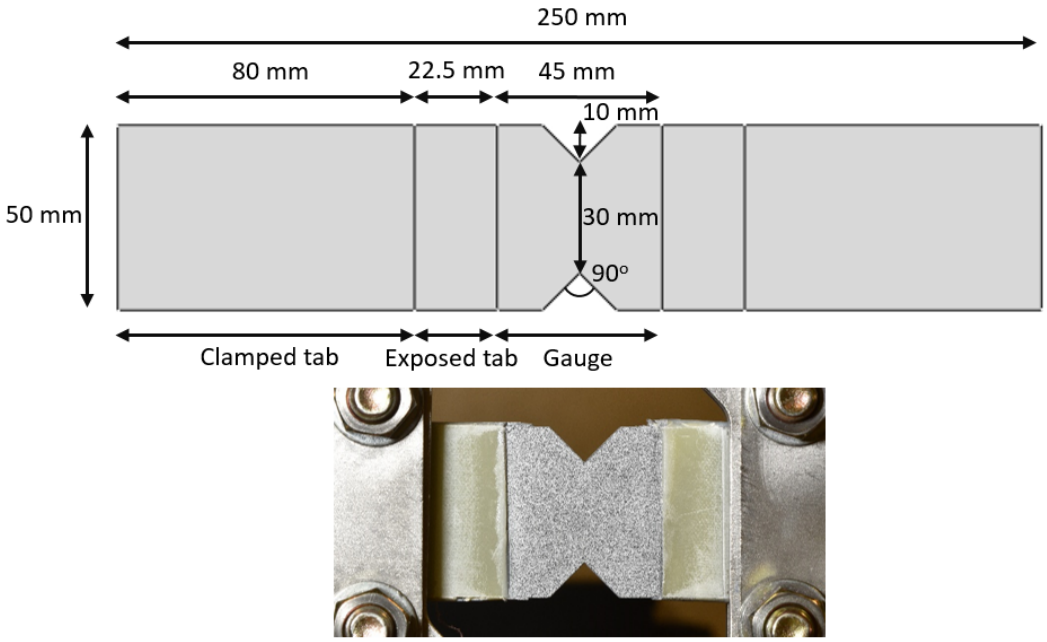

Figure 3.6: Final design of specimen

second moment of inertia would increase significantly, and load bearing capacity as well. To implement this solution, it is important to calculate the trade-off between the gauge length and cross section area for the optimal values. After performing several FE model and following specimen design from Yao *et al.* [39, 40] as guidelines, it is decided that the tab can be extended to cover a quarter of the gauge length from each end.

From Fig. 3.5, three notch depth designs are 15 mm, 10mm and 5 mm. The model shows that 5 mm is not deep enough, leaving 15 and 10 mm left. While 15 mm works, the notch region would be even larger than the middle cross section. In the end, 10 mm deep notch is the best design. By leaving the remaining 30 mm of neck area, more failure behaviors can be observed. With all of the dimensions fully analyzed for proper functionality, Fig. 3.6 shows the full final design of the specimen.

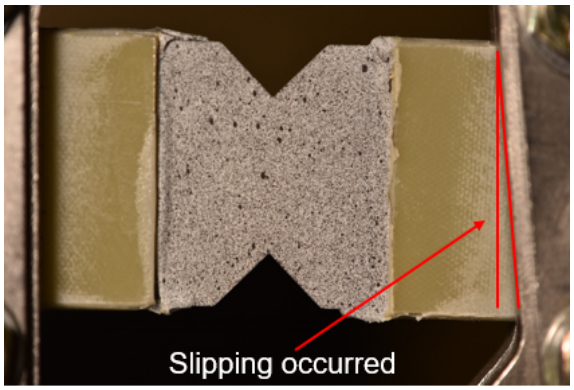

(a) Slipping during shear test with specimen loaded horizontally

(b) Bolt's indentation causes bending load

Figure 3.7: Problems with default friction clamping

3.2.3 Resolve Issue of Slipping During Test

In the past, the Arcan Fixture was made using stainless steel for durability. The outer surface is extremely smooth. The known proper way to clamp the specimen is to wrap a piece of rough sand paper around the specimen for better contact, then clamp it in the fixture by tightening six bolts to a measured torque of 130 Nm, or 95 ft-lb each [39, 40]. The method worked well for testing weaker composite like glass fiber laminates. However, it has come to attention that in the case of carbon fiber, slipping still often occurs.

During the trial runs using thin QI, about half of the tests show slipping. This behavior is clear when performing the shear test (Fig. 3.7a); it also happens in other loading angles, and even in tensile test sometimes. Figure 3.7b shows the evidence from the deformed tab when rotated off-axis and being pressed on to the bolt. The reason is that the friction from the sand paper is not strong enough to hold on to the clamp's stainless steel surfaces. Carbon fiber specimens were never tested with the Arcan fixture before. Therefore, this was not accounted in previous studies, during which materials failed before reaching maximum friction load. When slipping happens, the orientation of the specimen with respect to the loading direction changes. That would result in the specimen being under unintended

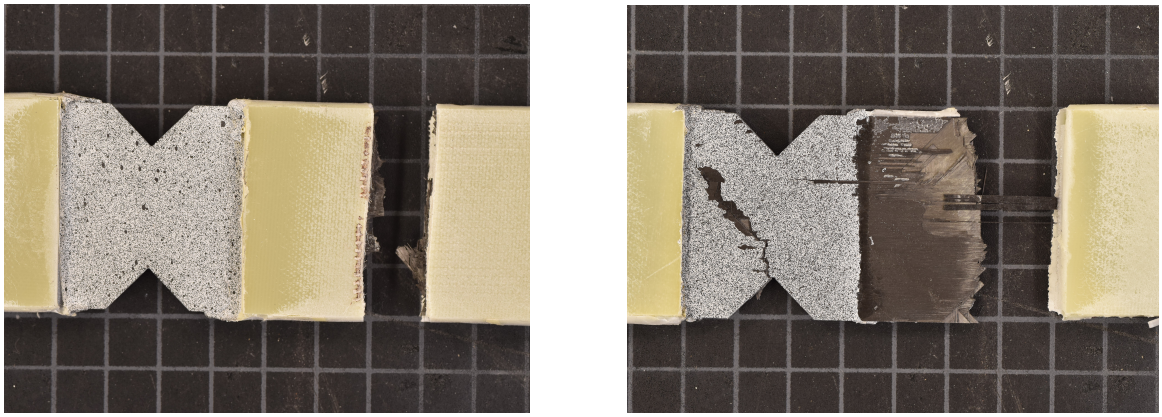

(a) Complete shatter at tab

(b) Premature debonding of epoxy and damage at tab

Figure 3.8: Broken specimen at the clamping border due to over-tightening

loading configuration and inaccurate reading of load and strain.

There are several approaches to this problem. Since the slipping rate is about 50%, it was proposed to simply perform twice as much tests to pick out the non-slip results. This would not be an efficient solution, since there would have to be twice as much time spent on manufacturing and testing. Furthermore, testing DFCs would have higher load, because of thicker specimen, so slipping would even more likely to occur.

It is decided to either increase clamping force or improve the grip surfaces. Increasing clamping force is easy to achieve. By simply applying higher torque, the clamping pressure would increase and so would frictional capability. However, during several trials, even with 150 ft-lb of torque and although with a lower rate, slipping still occurred. With 150 flt-lb, commercial tool's capacity is reached. Furthermore, due to high torque, the tabbed region of specimen can be crushed, causing damage at the clamping border Fig. 3.8, which eventually leads to failure at the fixture base. For those reason, simply applying higher torque would not work.

To improve the grip surface, the most certain way is to use physical grips, not friction. This will involve machining teeth onto the metal surface in grid patterns. However, the

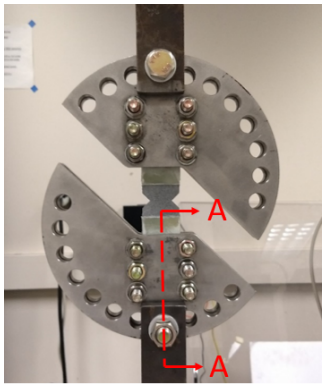

(a) Past setup does not have much tolerance for new implementation

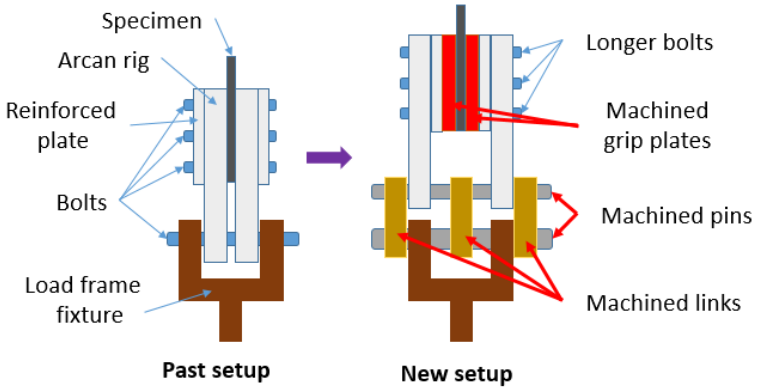

(b) A-A section of the fixture: Components with red arrows are steel grip plates, links and pins to be machined

Figure 3.9: Schematic layout of the new Arcan fixture steel grips and extensions

fixture's design is not suitable for machining grip patterns. Stainless steel is not durable and does not have high wear resistance. Even with machined patterns, the teeth will get worn out fast when used with hard materials like carbon fiber and fiber glass. The solution is to machine the grips onto extension pieces instead (Fig.3.9b, 3.10b). The extensions are made from tool steel, which has high wear resistance. Since the load frame's mounting system were not designed to fit these additional pieces to the Arcan fixture, extension to the mounting system would also have to be manufacture to accommodate the new setup as in Fig. 3.9. In total, an extension set of 14 steel pieces will have to be manufacture. After some trial runs, the new system shows significant improvement in slipping control.

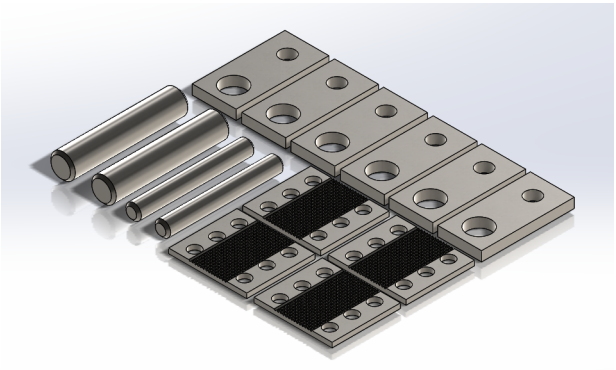

(a) Design of 14 components for the extension set

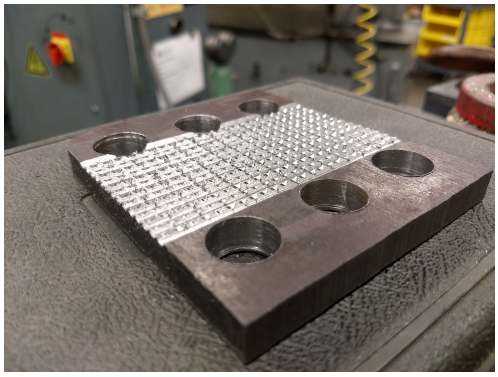

(b) Surface of machined steel grip plate. The manufactured grip plates eliminated the problem of slippage

Figure 3.10: Manufactured steel components

Chapter 4

EXPERIMENTAL RESULTS

With the Arcan fixture fully modified, the next step is to conduct multi-axial tests. The tests are performed with five different angle configurations: 0° / 36.5° / 49° / 62° / 90°. As a baseline to compare with DFCs' result, $[0/45/90/\text{-}45]_{2S}$ QI specimen are also tested as control data. The specimens are tested using Instron 5585H load frame. The test is displacement controlled, with the extension rate of 1.78 mm/min. Deformation data is collected using DIC imaging spontaneously. Between three and five specimens are tested for each angle configuration to ensure validity.

From the load data acquired from the Instron, the tensile and shear components can be computed from the uniaixal loading using simple trigonometry relations in Eq. 4.1,4.2. The loading angle in this study is measured as the angle made from the axis of loading and the specimen's longitudinal axis like in Fig. 4.1. Hence, 0° load angle means pure tension, and 90° means pure shear load. In this study, the loading direction of the experiment will always be on the y axis of x-y coordinate. The 1-2 coordinate denotes the specimen body coordinate.

$$\begin{aligned} P_{Axial} &= P cos\theta \\ P_{Shear} &= P sin\theta \end{aligned} \tag{4.1}$$

$$\begin{aligned} \sigma_N &= \frac{P_{Axial}}{\text{Cross area}} \\ \tau_N &= \frac{P_{Shear}}{\text{Cross area}} \end{aligned} \tag{4.2}$$

Figure 4.2 contains all of the load-displacement curves obtain from experiment. As mentioned above, DFC specimens are made to be 3.3 mm in thickness, but QI layup is only 2.4 mm thick. Therefore, DFC typically has higher load than QI. As the loading angle

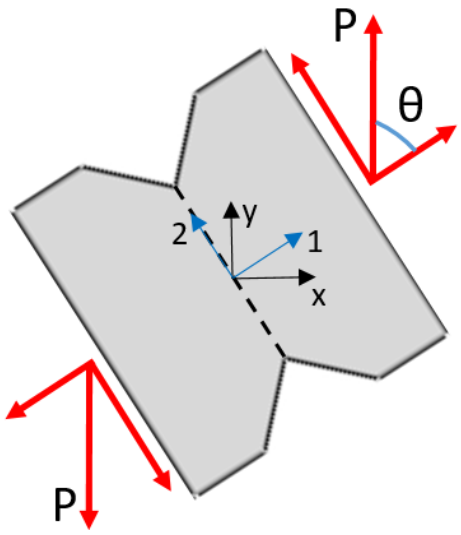

Figure 4.1: Tension/Shear load component

changes from 0° to 90°, shear load increases, which causes micro damages in the matrix system. This create non-linear behavior, and as a result, flatten the load curve. For both QI and DFC specimen, the curves are very linear with similar peak loads between attempts in pure tension. However, as the loading angle increases, the slope of linear region becomes smaller. Furthermore, the non-linear region appear even more strongly. For 90° angle, it can be difficult to identify the linear region, and when the non-linear effect take place. Looking at QI 90°, it would also be possible that the effect shear happen right after few millimeters of displacement.

When examining the linear slopes, QI curves in general are quite consistent. Most of the specimens even also follow the same non-linear paths. On the other hand, the slope obtained from DFC may lie within a range for each angle, and it seems that they overlaps. While 0° slope is quite distinct, some slope results of 36°, 49° and 62° practically coincide. The differences between them would be when the non-linearity take place or peak load. Furthermore, the non-linear effect observed in DFC also seems to be prolonged due to platelet damages. Due to the randomness of the platelets, failures may not happen in a single instance. It can be subdued thanks to the switching angles between platelets. When

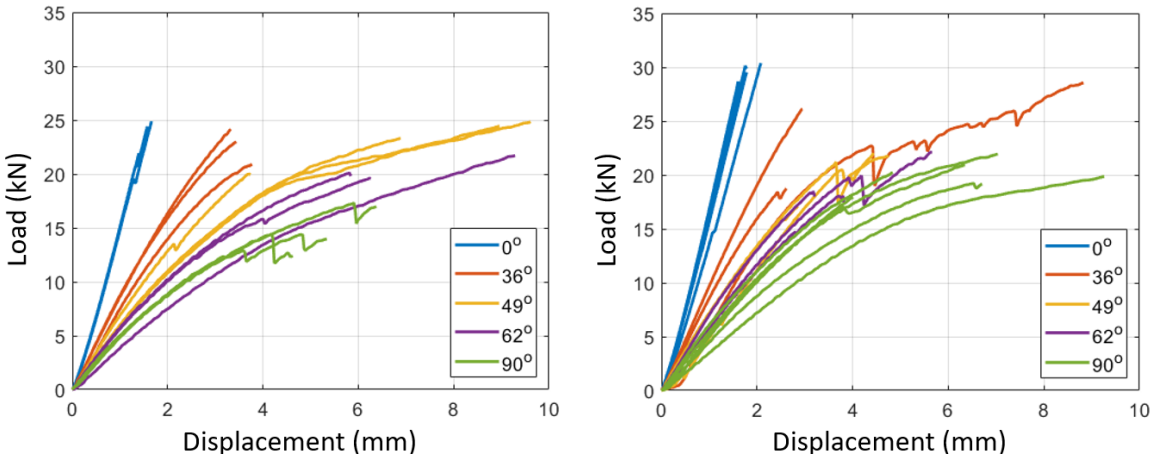

(a) QI specimens

(b) DFC specimens

Figure 4.2: Load displacement curves for all angles

that happen, there is a drop in load, but eventually recover. This mechanism increases peak load reading, and causes jagged curves. Certainly this behavior is not observed in QI specimens.

4.1 Examine stress envelope

After testing QI and DFC specimens in all angles, the maximum tensile and shear stress envelops are obtained (Fig. 4.3) with quadratic fitting applied. The envelops' shapes are very different. QI envelop covers the entire DFC envelop and beyond that. The far end of QI envelop lies about 62° specimens. As for QI, the tip of the envelop may be right at 90°.

$$Work = \frac{1}{2} P_{peak} x_{peak} \tag{4.3}$$

$$E_{total} = \int_0^{x_{peak}} P(x)dx \tag{4.4}$$

$$E_{dissipate} = E_{total} - Work \tag{4.5}$$

$$e_{dissipate} = \frac{E_{dissipate}}{\text{Gauge Volume}} \tag{4.6}$$

$$\lambda = arctan \frac{\tau_N}{\sigma_N} \tag{4.7}$$

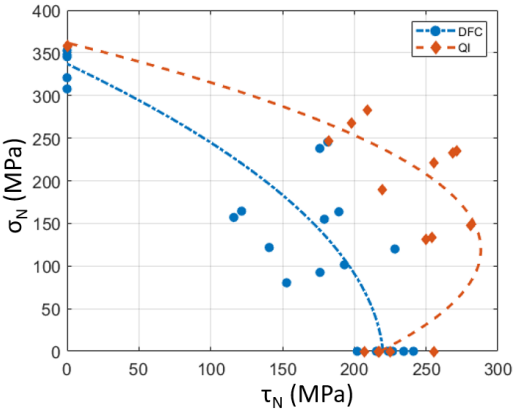

Figure 4.3: Stress envelop from experimental results

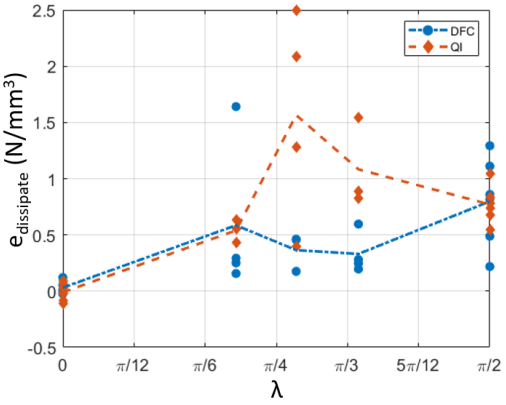

Figure 4.4: Dissipated energy as function of multiaxiality

Table 4.1 summarizes the average tensile and shear strength from the experiment. Regarding QI result, for most of the cases, it has higher strength than DFC. All of the QI's pure tensile (0°) specimens have the strength of 358 MPa with almost no deviation between attempts. Furthermore, it's noticeable that DFC specimens in tensile test all has lower strength than QI's, which is due to the nature of the material made of platelets. However, although sightly lower, most of them still have similar tensile strength as QI. In previous studies, DFCs have shown to have lower strength than QI, even with smooth specimens [32, 37, 48, 53]. DFCs' strength is typically about 50% of QI. Therefore, in this experiment, DFC's strength having a close match to QI is not expected. It is speculated that this is due to the size effect of DFC. On this scale, the meso-structure of DFC is on the same order of the specimen's size, and that exhibits strong size effect. This would require further investigation in the future works.

Overall, as the envelops showing, it is certain that under mixed mode loading (36.5° / 49° / 62°), QI outperforms DFC. Multi-axial loading results for DFC have low consistency, with the difference compared to the average ranges 15-20%. Despite being more consistent, QI results may still vary as much as 10% in some loading angles like 49°.

However, the result in pure shear does not follow the same trend as of other angles. On the stress envelop, the data points of QI and DFC scatter in a same range. This trend

is very similar to of pure tension, with the exception of wider range of deviation in data scattering for both materials. Furthermore, their average pure shear strengths are very close to identical. In a way, it means that DFC can provide just as much strength as QI when subjected to pure shear condition. However, just as DFC's unexpected tensile strength. The measure shear strength may be influenced by size effect.

Angle θ (deg)	QI Tensile (MPa)	QI Shear (MPa)	DFC Tensile (MPa)	DFC Shear (MPa)
0	358.07	N/A	334.84	N/A
36.51	265.40	196.34	201.20	148.78
49.18	219.36	253.73	146.74	169.73
62.31	137.47	261.63	98.58	187.59
90	N/A	224.34	N/A	223.87

Table 4.1: Average ultimate strength of QI and DFC in all angles

When examine the energy dissipated per specimen volume (Eq. 4.3-4.6) according to the multiaxiality (Eq. 4.7), similar patterns can be observed (Fig. 4.4). When multiaxiality is 0, it would be pure tension. Pure shear is when λ equals $\pi/2$. The energy dissipated in pure tension is almost none. This matches with the experiment behavior. Since the failure is very brittle-like, there was no chance for energy to dissipate. As for pure shear, QI and DFC share similar average values. This means there is not much different in the energy dissipated in pure shear for both QI and DFC. However, the DFC shows wider range of deviation compare to QI, in both minimal and maximum value. Some DFC specimens show greater dissipation of energy compared to QI.

For the mixed-mode cases, there are a lot on inconsistency in data. QI has very high deviation in some cases. With such scattered data points, the determined average values are not very precised to make any conclusion. On the contrary, DFC shows good consistency, with an exception of outlier. Overall, the trends show that DFC has lower energy dissipation than QI. QI seems to have a highest dissipation amount at certain multiaxiality. On the

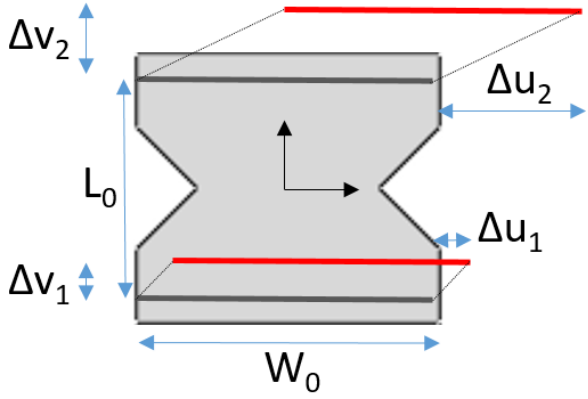

Figure 4.5: Spatial deformation of gauge area measured on gauge lines (black/red)

other hand, DFC shows consistent amount of dissipation throughout all mixed mode cases. As confirmation, just like the usual responses in strengths, these results still requires further investigation in the future.

4.2 Examine tension and shear components

As mentioned above, the tension and shear load can be computed from Eq. 4.2. The strain is calculated from DIC deformation. To calculate strain, the displacements of two gauge lines on opposite ends of the gauge area are measured (Fig. 4.5). Then, the difference in displacements of those two lines is divided to the nominal length to get strain data. The nominal length is the average distance between the aforementioned lines at the beginning.

The strain computed using the difference in longitudinal displacements (1-direction) is the tensile strain ϵ_{11} (Eq. 4.8). In the pure shear condition, there would be only lateral movements (2-direction) that contribute to shear strain, while the displacement in 1-direction is negligible. With the problem of specimen rotation during testing eliminated, and with the specimen's brittle manner of failure, displacement in 1-direction related to shear can be neglected. Furthermore, analysis on the experimental data shows that the displacement in 1-direction is two to three orders of magnitude smaller than 2-direction's. Therefore, as a simplification, shear strain γ_{12} is the result of lateral displacement only (Eq. 4.9). This γ_{12} is engineering strain, which differs from normally used true strain obtained from Eq. 4.10.

Since the purpose of this study is not to characterizing the material's properties, true strain computation is not necessary.

$$\epsilon_{11} = \frac{\Delta u_1 - \Delta u_2}{L_o} \tag{4.8}$$

$$\gamma_{12} = \frac{\Delta v_1 - \Delta v_2}{L_o} + \frac{\Delta u_1 - \Delta u_2}{W_o} \approx \frac{\Delta v_1 - \Delta v_2}{L_o} \tag{4.9}$$

$$\epsilon_{ij} = \frac{1}{2}(u_{i,j} + u_{j,i}) \tag{4.10}$$

4.3 Examine morphology

Generally, the failure in QI starts at the notch and then spread to the other end. Most of the time, the crack path would reach the opposite notch tip. Nevertheless, the path is generally straight across the specimen, and specimen breaks into two. Often times there are fibers in $\pm 45^\circ$ ply that did not fail and get pulled out instead (Fig. 4.6a). In a few occasions of mixed loading and pure shear, there are secondary failure at the clamping border that happen at the same time or later than notch failure.

There are few key differences between tensile and shear failure. On the large scale, delamination usually happens in pure shear. This can be as small as a few millimeters away from the failure site (Fig. 4.6b middle), or all the way to the tab border (Fig. 4.6b right). Usually, delamination happens at the outer surfaces. The only case where it happens from within for QI would be $\pm 45^\circ$ being pulled out.

There are other features under microscopic level. Under pure tension, 0° ply failure has teeth-like marks, and the path is usually straight (Fig. 4.7a). In some cases, the path may travel 45° instead, but eventually curve back and arrive at the notch site. On the other hand, 0° ply under pure shear breaks cleanly, leaving a smooth line with slight curve (Fig. 4.7b). However, the curve is minimal, and the path is generally straight. Unlike pure tension, the curve does not travel diagonally but instead create diagonal stair case pattern. The shifting in heights between steps create splitting in the 0° ply. Some of those splitting grows and delaminate on the macro scale.

(a) Tensile failure

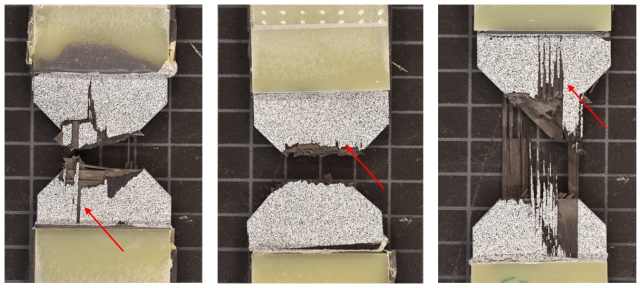

(b) Shear failure usually has delamination

Figure 4.6: Broken QI specimens of pure tensile and pure shear loading

The failure patterns of ±45° plies have some similarity with 0° ply. It was expected that the failure of the ±45° plies under pure tension would be similar to pure shear 0° ply, and same for their counterparts. However, the morphology shows differently. For pure tension, failures are typically teeth marks (Fig. 4.8a). The path may run across the notch, but can also run normal to ply direction, which is diagonal to the specimen. On the other hand, failures in pure shear often leave a clean cut (Fig. 4.8b). The path of failure can also be either across the notch or the ply. Under pure tension, both positive and negative 45° ply would be applied the same load in the same direction, and therefore have similar failure patterns. In the case of pure shear, due to side-way loading, theoretically one ply would be subjected to tension load, while the other would be under compression. Therefore, that would make two different failure mechanism. However, there are still no difference found in the failure patterns between the angles. Regarding 90° plies, there are no distinct traces

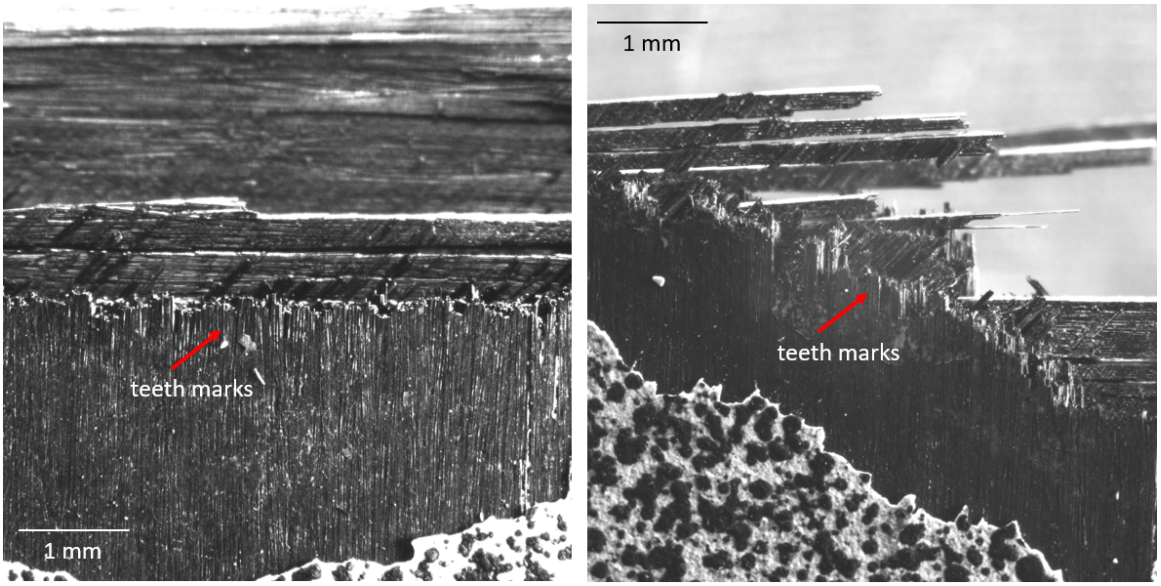

(a) Pure tension has teeth marks on 0° ply

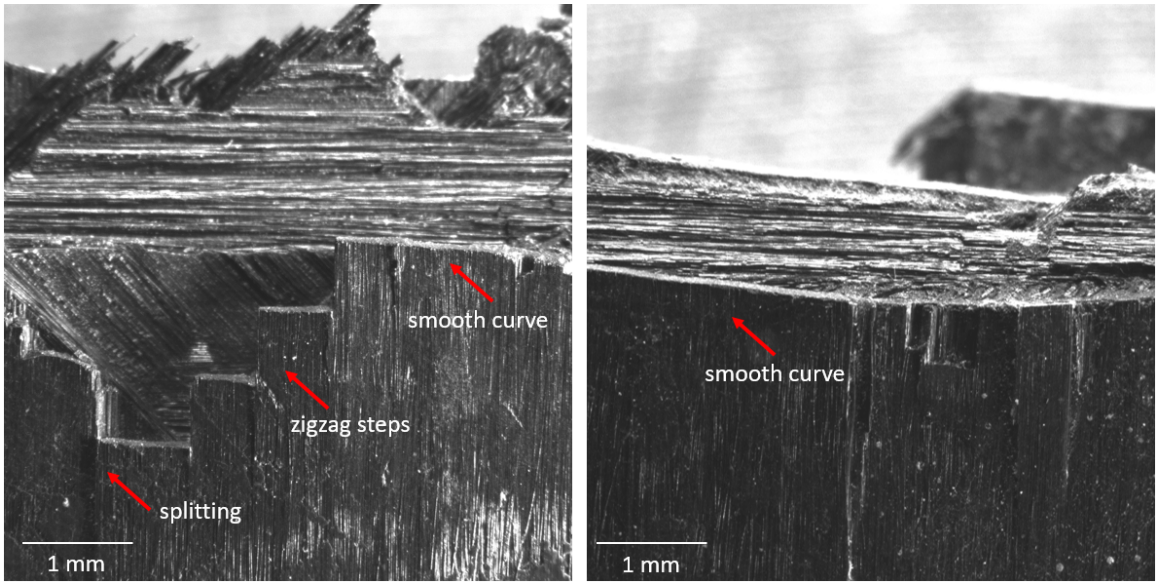

(b) Pure shear has smooth break line and splitting on 0° ply

Figure 4.7: QI specimen, pure tensile and pure shear failure on 0° ply

between different loading condition. The failure is often due to fiber breaking cleanly and on the same height with of the plies' failures, making it hard to identify.

When the specimen is loaded in off-set angles, it would be subjected to both tensile and shear load. The failure of 49° loading case in Fig. 4.9a contains both the teeth marks feature of tensile, as well as smooth curve and step-like breakage of shear load. Shear and tension failure can happen at two separate locations on a same specimen. However, there are also occasions of them being mixed together. The shear failure on 0° ply may create a slight curve, which is actually made of teeth marks from tension along the line (Fig. 4.9b). The ratio of tensile to shear mechanism depends on the loading angle. As loading angle shift towards 90°, more curves and delamination would occur.

Unlike QI, DFC exhibits similar failure morphology in all loading direction. From Fig. 4.10, the failure may result in more than two broken pieces; and often times, the path would stray away from the notch region end up close to the tab borders. Compare to QI, the region of fracture is larger, and more delamination. On the micro scale, the failures shows fiber splitting, fiber breakage in both teeth marks and smooth curve (Fig. 4.11). Those features appear in all loading angles, and it is noted that there are more teeth marks than smooth curves. Step-like patterns sometimes occur but also hard to identify since they are very similar to the platelet's corner. Furthermore, that feature requires a wide region of UD. Therefore, the narrow width of platelets may limited the chance of it happening. Teeth mark feature appears on most of the platelet tips. Regardless of the loading, the teeth marks appear in all directions. Along of teeth marks, there are also a lot of fiber splittings. Splittings happen within a platelet. In some cases, splitting stops when encounter an offset neighbor platelet. However, it can also break the neighboring one along with its path.

While QI has a change of ratio between tensile and shear failure according to loading angle, that does not apply to DFC. However, that would mean the same distribution and types of failure mechanisms happen on both pure tension and pure shear but result in different material strength. It's speculated that the difference in strength comes from the order of failure happened. During pure tension, there is little displacement, and the behavior is quite still in the elastic zone. Therefore, it can be guessed that platelets closer to loading direction hold most of the load. After those load bearing platelets fail, the rest would also

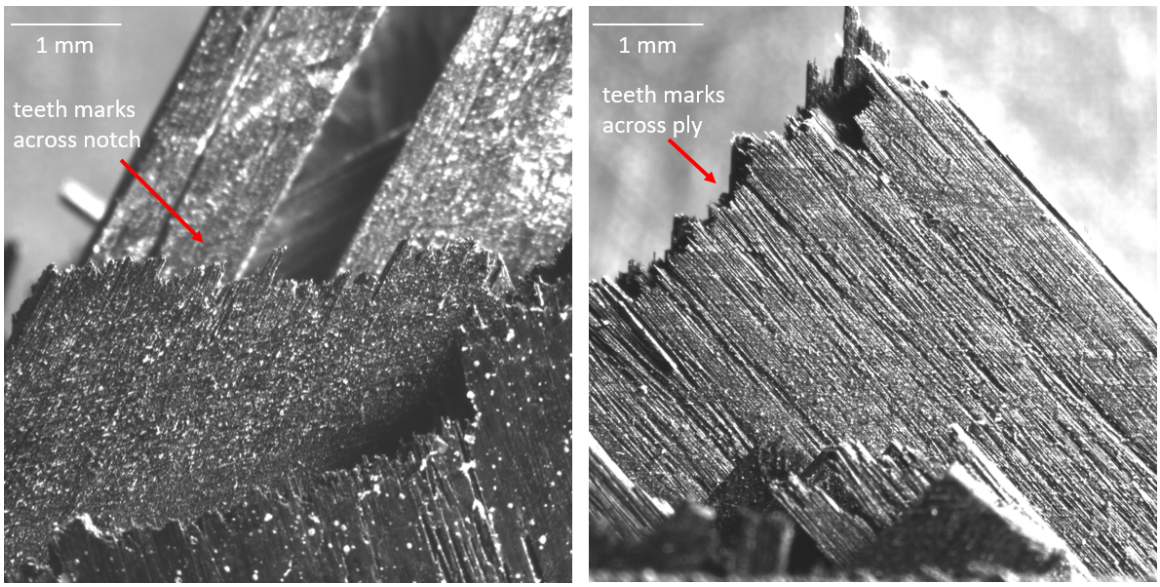

(a) Pure tension has teeth marks on ±45° ply

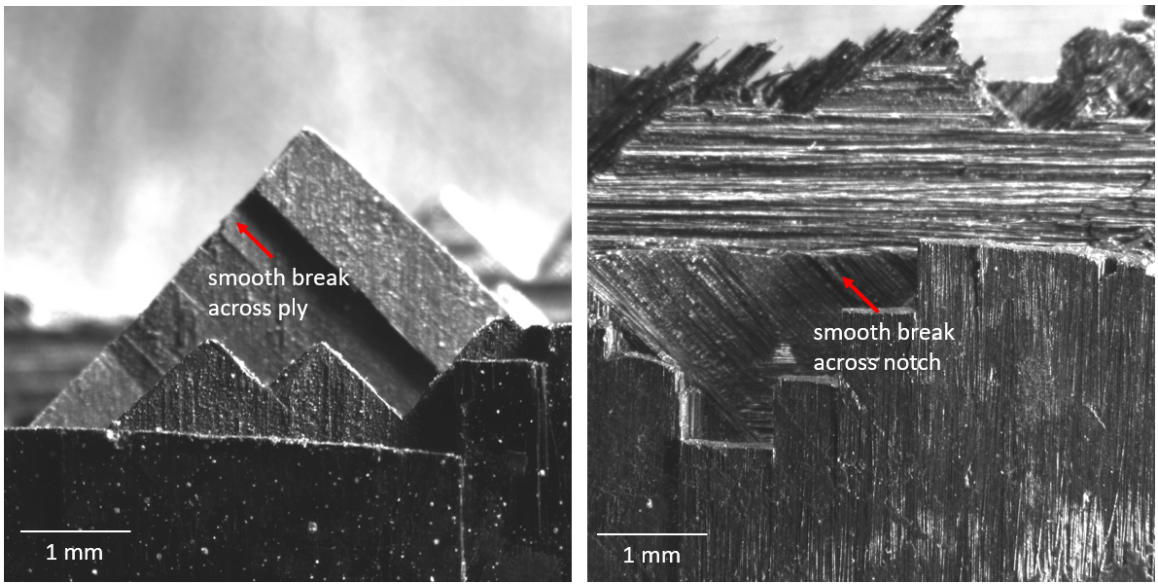

(b) Pure shear has smooth break line on ±45° ply

Figure 4.8: QI specimen, pure tensile and pure shear failure on ±45° ply

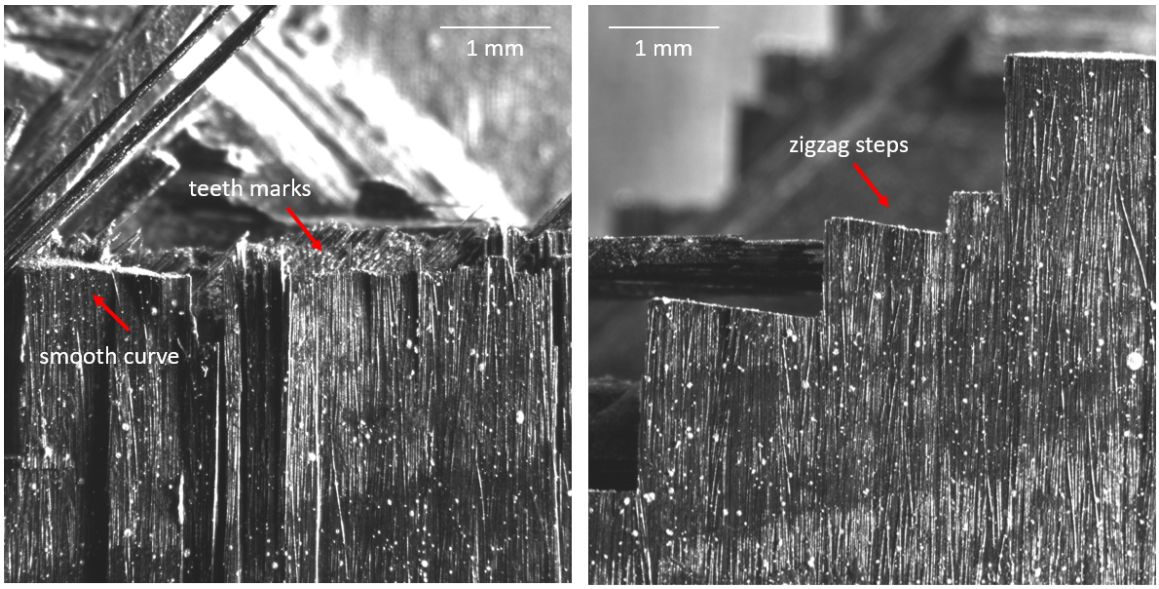

(a) 49° failure

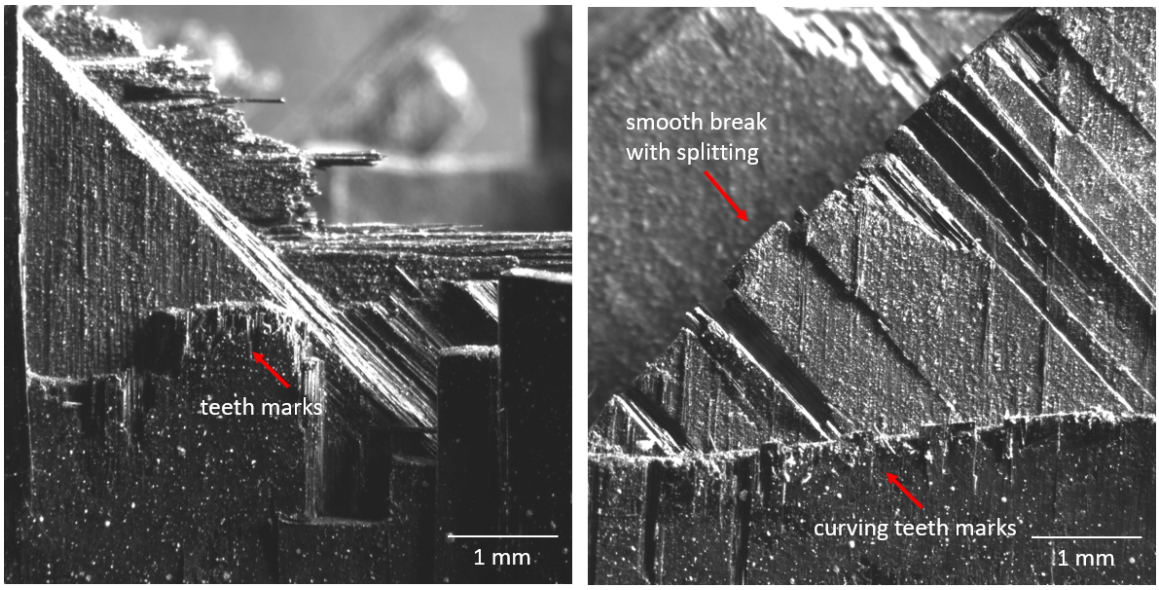

(b) 62° failure

Figure 4.9: QI specimen, failures of mixed-mode cases

Figure 4.10: Broken DFC specimens of 0° / 36° / 49° / 62° / 90° loading angle

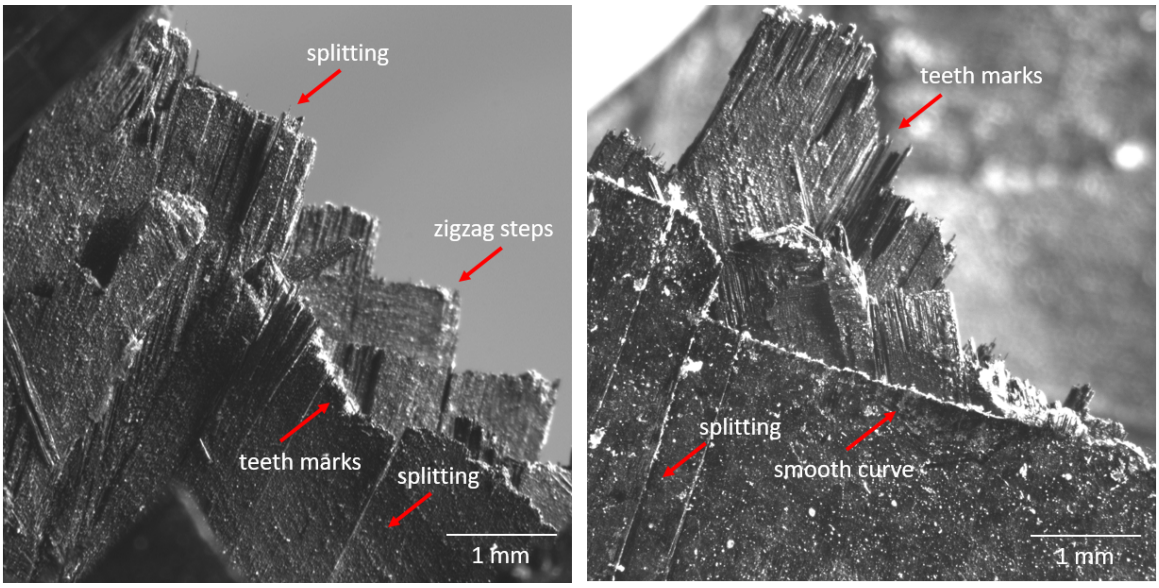

Figure 4.11: DFC exhibits both shear and tensile failures for all loading cases

in just an instance due to sudden release of displacement restriction. In pure shear, what happens might be the other way around. Platelets in shearing direction would fail first due to matrix deformation, and then gradually to platelets aligned with the specimens. When failure happens in the mention order, it would slowly release energy and allow more displacement/deformation in the structure. As a compensation, the stiffness would gradually decrease, and the peak load can only be counted on the remaining platelets that are closer to the loading direction.

Chapter 5

FINITE ELEMENT ANALYSIS

The finite element model is constructed using commercial software Abaqus (6.13) [3]. The material's parameters follow T700 prepreg's specification [12] (Table 5.1). There are multiple steps in the expected method of approach to a fully implemented DFC multi-axial FE model. First, a QI specimen model is made as the foundation to match the loading configurations. The appropriate failure modes are implemented to capture the non-linear behavior and strength. The experimental results of QI help validating the FE model. The DFC model, which is basically based on randomized orientation of material sections, will be adapted into the QI model. Both the QI and DFC model then will be validated using experimental results.

Parameters	Symbol	Unit	Room Temperature Value
0° Tensile Modulus	E_1	GPa	125
90° Tensile Modulus	E_2	GPa	8.41
In-plane Shear Modulus	G_{12}, G_{13}	GPa	4.23
Out-of-plane Shear Modulus	G_{23}	GPa	3.7
Poisson's Ratio	ν_{12}	-	0.31
0° Tensile Strength	F_{1t}	MPa	2172
90° Tensile Strength	F_{2t}	MPa	44.3
0° Compressive Strength	F_{1c}	MPa	1448
90° Compressive Strength	F_{2c}	MPa	199
Longitudinal Shear Strength	F_{12}	MPa	154
Transverse Shear Strength	F_{23}	MPa	86.2

Table 5.1: T700 model parameters

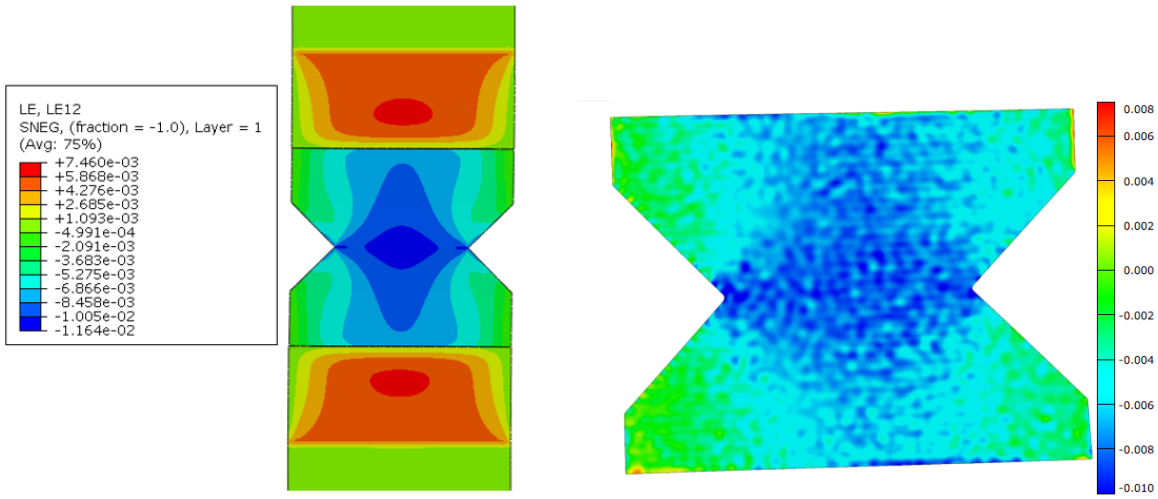

(a) Shear strain from FE model

(b) Shear strain from DIC analysis

Figure 5.1: Comparison of shear strain field between modeling and experiment

5.1 Examine elastic properties using standard solver

A conventional shell S4R is used with a homogenized composite layup section. The stiffness calculation for the FE result of the pure tension shows good agreement with the experiment, with an error of 0.02%. However, the stiffness of pure shear model is two times larger than the experiment. Troubleshooting for loading condition, data calculation, material properties, finite element principles and guidelines are performed to resolve this problem.

To compare with the testing result, one single method of calculating the stiffness is performed on both FE model and experiment to maintain consistency. With the pure tension stiffness comparison having such high precision, it would certainly not be due to DIC imaging or strain formulation. The next step is to inspect the development of strain and reaction force values over time. Through increment-wise inspection, it shows the average displacements of top and bottom gauge lines from DIC and FE model are consistent with each other. Figure 5.1 shows that the strain field obtain from DIC and FE are similar. With the displacement confirmed, it means that the reaction force from the FE is twice as high than expected. Since the experimental load data is acquired using Instron sensor, no

post-processing is needed. It means that the force response of the FE model is inaccurate. And thus, the next step turns to examine the Abaqus implementation of the shell element used.

The shell element used is S4R, which is a general, all purpose element for most shell problem. According to Abaqus documentation, S4 element also provides good accuracy to in-plane bending problem [3]. Therefore, it would also be suitable for in-plane shear problem. The element also does not require hourglass control, the effect that makes the model stiffer than expected. However, as a precaution, fine meshing is still applied to reduce to the likelihood. Finer mesh is also applied at the notch region and tips to make sure the stress concentration is fully captured. As for the element section, there are no difference in using composite layup section or normal material section. The same can be said to using different material definition like lamina, engineering or orthotropic defined parameters.

The loading condition is the third point of inspection. It is noted that for a perfect pure shear test, no rotation would involved. So in theory, all rotational degree of freedom should be fixed. However, during the experiment, Arcan fixture and extensions are all held up using pin joints. For small deforming cases, the effect due to rotation can be neglected. However, with large deformation due to non-linear behavior of matrix and specimen's size, the fiber alignment would eventually rotate toward the loading axis. When this happen, the specimen is no longer under pure shear condition but a mixed shear-tension load instead [38]. Therefore, to avoid this condition, usually shear specimens are small. The gauge length between clamping region can be as small as a few millimeters. On the other hand, the designed specimen has 80 mm of gauge length, which would amplify the effect of misalignment. Since the purpose of the FE model is to fully replicate the experiment, modification is needed to include rotation about the z-axis.

At first, the rotation is suspected to be dependent on the geometry and mass of the specimen or the fixture. Since the fixture has a lot of mass, the location of the fixture's center of mass (CG) may determine the direction of rotation, as well as its magnitude. Therefore, different loading on different pin location may results in different rotation. This suspicion come from the fact that the specimen's CG and the fixtures' naturally lie in a straight line, but do not coincide with each other.

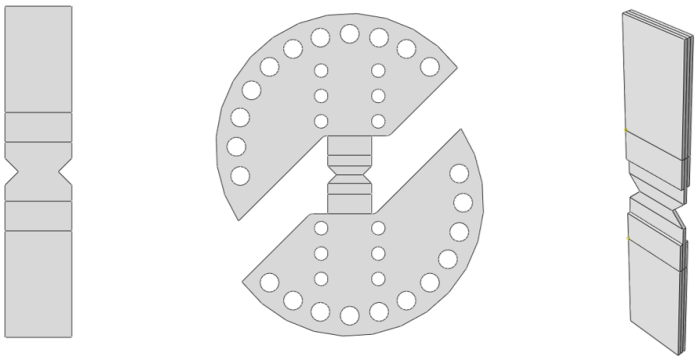

(a) Specimen-S4R (b) Arcan system-S4R (c) Specimen-SC8R

Figure 5.2: Implemented FE models using different geometries and element types

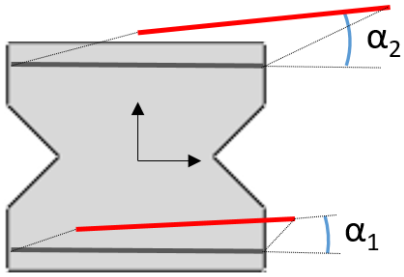

Figure 5.3: Body rotation of specimen

The initial model only has the deformable, exposed region of the specimen. To test the rotation, two new versions with a full size specimen and a full Arcan system are tested (Fig. 5.2). The region of clamping and fixture for both models are assigned as rigid body. A full specimen model using SC8R element is also made. However, the result shows little changes between models. The rotation calculated from the models are on the order of 10^{-6} rad, which is minuscule (Fig. 5.4a). Using DIC, the rotation is also calculated by measuring average rotation of the bottom and top gauge lines in Fig. 5.3 following Eq. 5.1. Figure 5.4b shows that the rotation develops linearly with shear strain until failure. However, the largest rotation is only 0.03 rad, or roughly 1.7°.

$$\alpha_{avg} = \frac{\alpha_1 + \alpha_2}{2} \tag{5.1}$$

Through visual comparison between the initial and final frame of DIC in Fig. 5.4c, the final angle of the specimen is also measured to be about 1.5°. [38] did some experiment using Arcan fixture. In their experiment, they also noticed fiber rotation of 0.5-1° linearly at the beginning. The difference in rotation growth between theirs and the current experiment is likely due to different apparatus setup. In the end, after confirming with experimental value, FE model and literature, the effect of rotation is deemed insignificant.

After checking all sources of error in material's property, element parameter and boundary condition, none are found to cause error in shear stiffness. Therefore, there is a possibility that standard solver may not be able to model shear behavior. When it comes to shear, large deformation can occur. From Fig. 4.2a, it can be observed that the stress-strain plot started curving right at the beginning. The linear elastic region may only lasted for that first few increments only. The non-linear curve may happen due to micro damages happen throughout that test, which cause large deformation. Therefore, the pure shear model would be continue to be improved using explicit solver.

5.2 Examine material strength and shear response using explicit solver with Hashin failure criterion

If the non-linear behavior in shear is due to the micro damages, that it would be important to implement the right model that take into account of those damage mechanics. As a starter, Hashin damage model is used [52]. The full specimen model using shell element S4R is implemented since there is no benefit in modeling the whole Arcan fixture. Shell element S4R was chosen over SC8R to reduce computational cost. The explicit model is only to capture the behavior to the peak strength. Therefore, non-quasistatic behavior and post-failure modeling will not be considered.

The first step is to match the strength of pure tension specimen from T700 (Table.5.1) specification. The experimental peak load is 25 kN. The initial Hashin damage model however only reaches 20 kN. The reason is due to of the lack of interlaminar damage mechanisms in the model. The section used is composite section that is consisted of 16 UD layers. How-

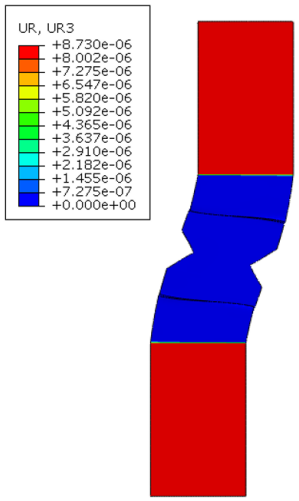

(a) Body rotation from FE model

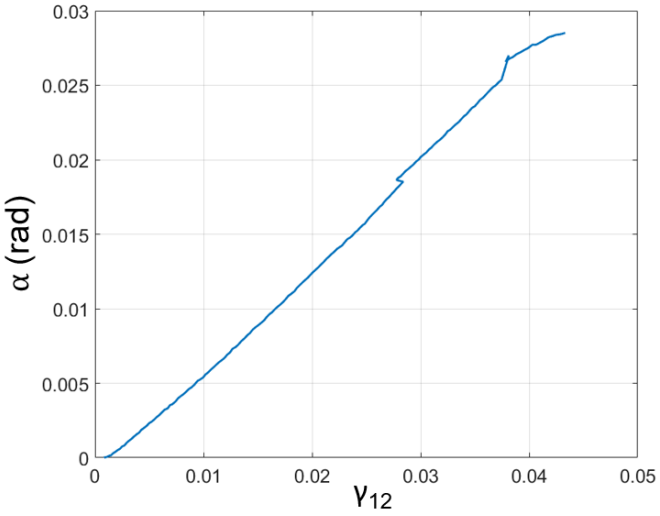

(b) Body rotation captured from DIC

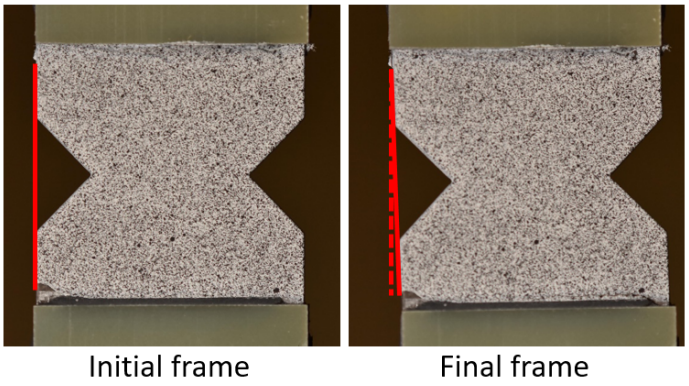

(c) Visual inspection between initial and final frame for body rotation

Figure 5.4: Body rotation from experiment and simulation

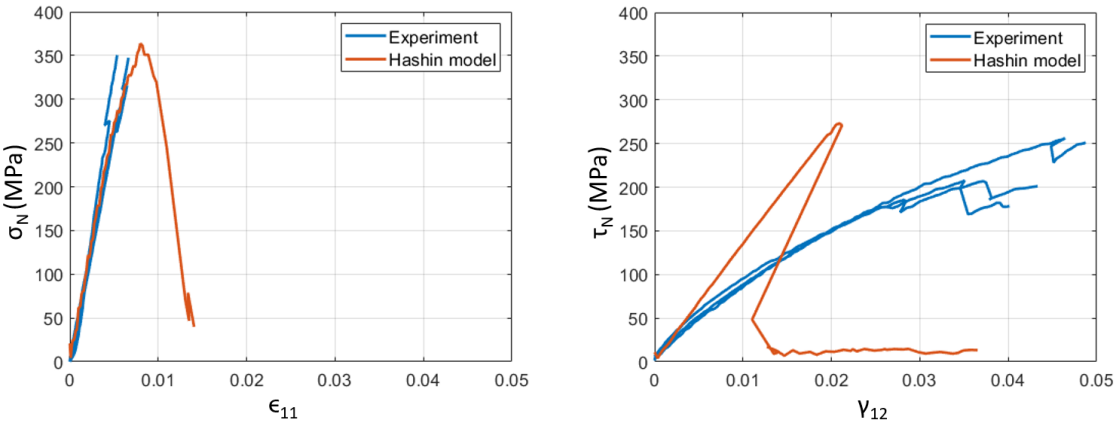

(a) QI Pure tension

(b) QI Pure shear

Figure 5.5: Stress-strain curves of QI pure tension and pure shear loading cases

ever, this approach homogenizes the fiber and matrix properties, which would not be able to model the interlaminar failure mechanisms. Since interlaminar failure such as delamination is very crucial, the shell section needs to be changed.

In the latest setup, the model replicates the full dimension of the specimen, including the clamping region. The specimen is made of a stack of 16 separated plies. Each ply is a single composite laminate using conventional shell element S4R. The model also has cohesive element COH3D8 with 0.001 mm thick between individual plies. These cohesive layers will ensure interlaminar failure mechanism such as delamination. In the stack configuration, the top surface of each cohesive layer is then tied to the bottom surface of the ply above. The top and bottom clamping region are assigned as rigid body, with the reference points positioned at the Arcan's pin locations for the corresponding load.

The new model predicts failure for pure tension at 26 kN at 0.4 mm displacement. The experiment result has peak load of 25 kN at 0.408 mm. From Fig. 5.5a, the stiffness obtained from Hashin model is about 0.41% error compare to the experiment's. With such accuracy, it shows that T700's parameters are appropriate, and delamination is one of the major failure mechanism. The model is also able to capture a lot of delamination at the center region (Fig. 5.6a). While delamination is modeled by discretizing individual layers

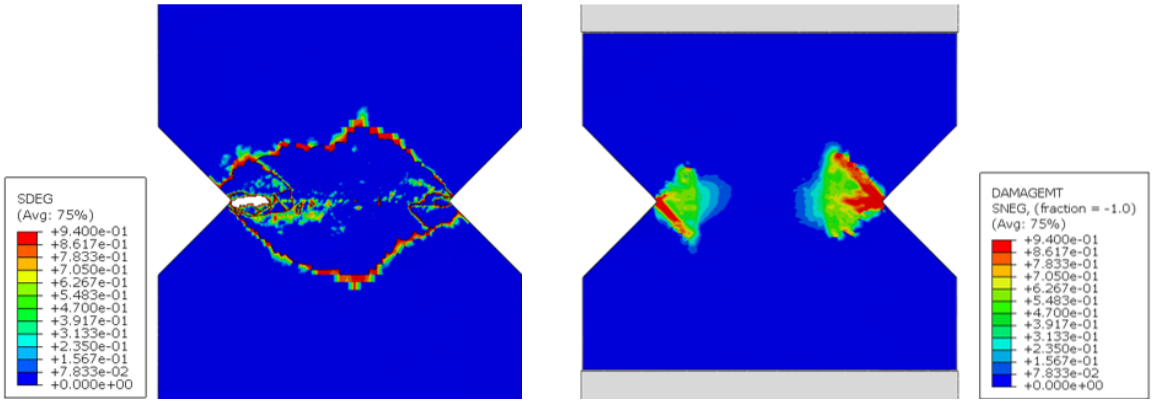

(a) Delamination (b) Matrix tensile failure on 45° ply

Figure 5.6: Hashin model of QI under pure tension

the bonding in between, the fiber and matrix is still homogenized in each ply. Due to existence of notches in the structure, there is likelihood of stress concentration at the notch tip. When this happens, to dissipate stress and blunt the notch tip, the fiber in the 0° ply would start splitting at the notch tip. This creates vertical splitting line normal to the notch tip, or so called splitting cracks. This cracks would penetrate through the plies. As it reach the 90° plies, it would dissipate energy by making more smaller crack surface along the fiber direction, which are called diffused microcracks. This crack and splitting is due to shear failure of the matrix between the fibers. Because of the homogenized section, Hashin criteria cannot differentiate shear across the fibers vs. shear along the fibers, thus cannot model the splitting cracks of the lamina. Instead, the Hashin model show failure of the matrix along the fiber direction on 45° ply (Fig. 5.6b). To model splitting crack failure mechanism using Hashin, it would require similar solution of separating individual plies, discretizing lines for crack path. However, this modification of meshing is not suitable for implementing DFC's generating algorithm. The implementation of splitting crack path is for the future work and thus not implemented in this study.

The second drawback of Hashin criterion is the incapability of modeling non-linear shear behavior. Since Hashin model cannot differentiate shear between ply's longitudinal and

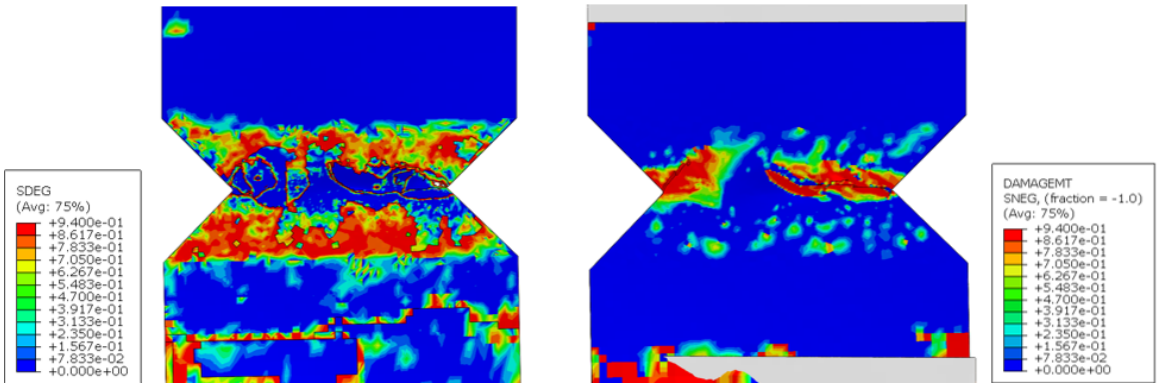

(a) Delamination (b) Matrix tensile failure on 45° ply

Figure 5.7: Hashin model of QI under pure shear

transverse direction, it would assume those two to be the same. With such assumption, there would be only complete failure of the element and no gradual transition of micro-damaging. In Fig 5.5b of pure shear model, Hashin model has a strong linear slope, and then snap back instability occurs. When examine the damage mechanisms, it is found that the model did not capture any failure at all throughout the whole linear loading response. All of the failures captures in Fig. 5.7 happens within a single increment of the analysis. In other words, the FE models QI as an extremely brittle material. Since shear behavior become non-linear in the very beginning, Hashin model does not match at all. As a confirmation, the model is repeated for other angles. The results are a combination of pure tension and pure shear. Just like pure tension and pure shear responses, tensile components show consistency in stiffness and similar behaviors to the experiment. Shear components have strong linear region and then snap back instability. The stress envelop obtained in Fig. 5.8 from all the angle configuration show that not only the values but also the envelop shape is not correct. This mean the failure mechanism is not fully modelled.

In the end, Hashin criterion is not suitable for modeling shear failure in QI specimen. Since this is a very complex behavior, it is necessary to implement models that can capture micro damages in material level. Unfortunately, Abaqus library does not have other failure

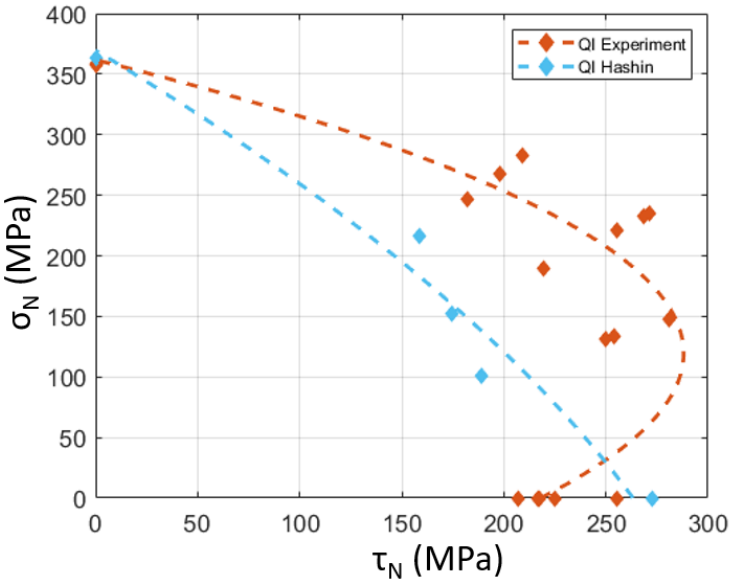

Figure 5.8: Stress envelop of experimental and Hashin model of QI

models that work better than Hashin's in this situation. Therefore, to capture the non-linearity, the right decision would be to implement other advance models using subroutine. However, the purpose of this study is not to model QI specimen but DFC instead. While Hashin criterion may not be a good option for QI, it may still fit for DFC. There is possibility that the non-linear behavior may be less relevant in presence of DFC's unique characteristic of randomization.

5.3 DFC model implementation with Hashin failure criterion

DFC model is adapted from Ko *et al.* [41, 42]. Overall, the DFC model generates platelets in random locations and orientations onto a predefined partitions or grids. The information of the platelets would then be saved in the material section of the elements that the platelet located on. The model only make thin plies of DFC to replicate the manufacturing process. The model doesn't consider the out-of-plane orientation of the deposited platelets. Therefore, to create a 3.3 mm thick model, the plies would be stacked onto each other with cohesive element in between to model delamination. In other words, DFC model has the

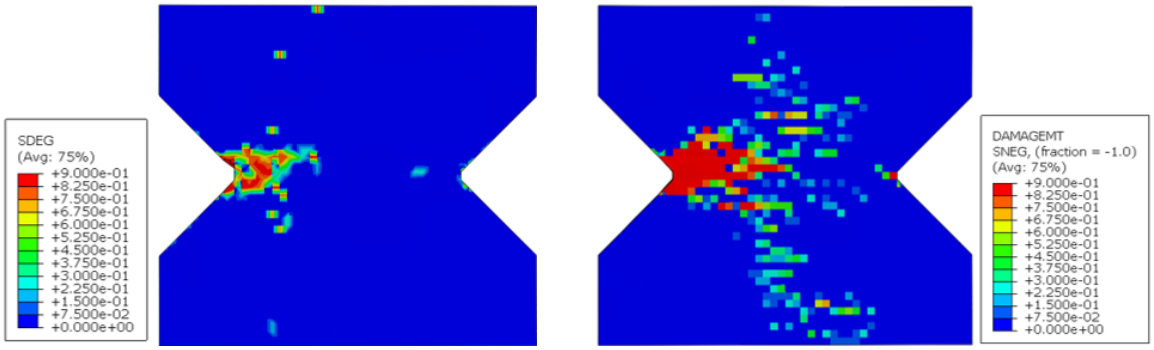

(a) Delamination (b) Matrix tensile failure

Figure 5.9: Hashin model of DFC under pure tension

same configuration as QI, with the only exceptions of number of plies for proper thickness, and unique layup section information such as in-plane orientation and material stacking order. And so, DFC model requires minimal accommodations from the QI FE model.

DFC model in both pure tension and shear show main mechanism of failure are delamination and matrix failure (Fig 5.9, 5.10). This agrees with the morphology results, of which fiber pull-out, matrix cracking and delamination often identified. On the first attempts of using QI specifications for DFC model, the strength of DFC is completely off from the experimental. Furthermore, it is observed that DFC model also behaves linearly under pure shear configuration. From that, it is suspected that the non-linearity does not necessarily comes from shear, but maybe from delamination. From plotting the stress envelop, numerical results show correct envelop shape, but with lower strength in both tension and shear. The next step is to calibrate the parameters of fracture energies of the platelet and cohesive element to match with pure tension and shear. With the strength properly calibrated in those two configurations, all of other angles are simulated, along with two additional angles of 12° and 76° to test the validity (Fig. 5.11). The result envelop matched with the experimental, in both shape and magnitude. From that, it is certain that the fracture energy of DFC is higher than QI. Furthermore, the correct envelop shape obtained is the proof that DFC model is able to capture the right failure mechanisms.

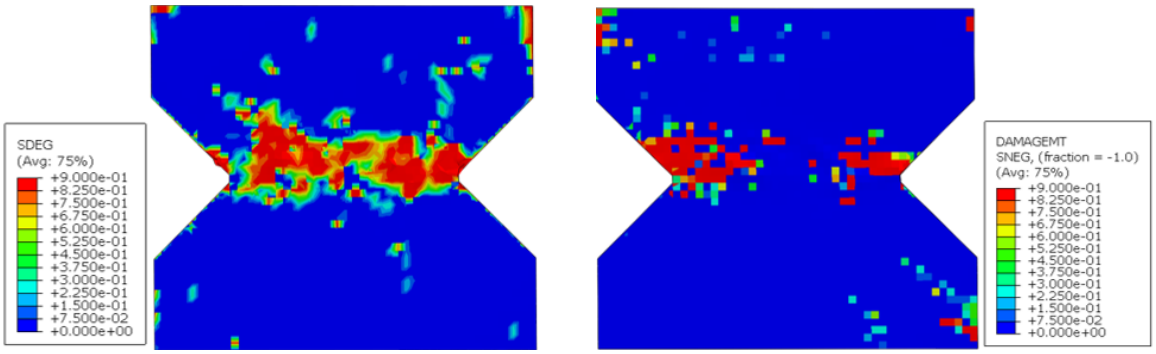

(a) Delamination (b) Matrix tensile failure

Figure 5.10: Hashin model of DFC under pure shear

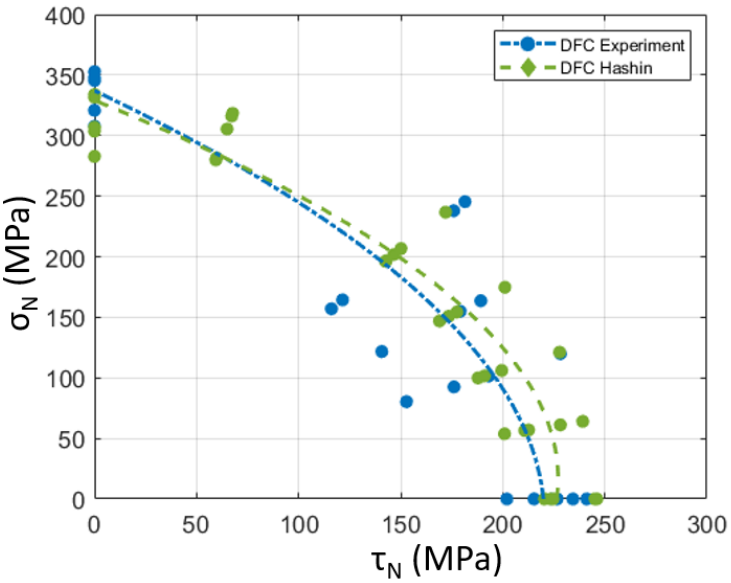

Figure 5.11: Stress envelop of experimental and Hashin model of DFC

Chapter 6

CONCLUSION

From this project, more knowledge about DFC has been obtained. The Arcan test system is originally adapted from Yao *et al.* [39, 40]. From that, the testing system then goes under significant adjustments and modifications. Thanks to that, the capability and capacity are enhanced to be able to perform test on not just fiberglass but also carbon fiber materials, and even with large size sample. As a result, multi-axial test on traditional QI and DFC specimens made from carbon fiber are conducted smoothly. This opens more possibilities for other multi-axial studies using the improved Arcan system.

From the experiment, both QI and DFC are tested, from which provides deep insights about their responses under multi-axial loading. Furthermore, the stress envelops of DFC and QI are clearly identified. Through analysis of the experimental data, it can be stated that DFC inherently has different envelop shape compared to QI. In a way, that means DFC is different from QI in stress response and damage mechanisms. In addition, DFC and QI seem to have similar energy dissipation under pure tension and pure shear. However, DFC has lower dissipation capability under mixed mode loading. While the mentioned trends are observed with the available data, more tests are needed to have a more accurate judgement on this matter. Furthermore, the morphology of DFC and QI are well-captured, showing the failure mechanisms that took place. This serves as a qualitative evidence of the difference between DFC and QI's failure mechanisms. And on a side note, DFC showed unexpected strength that matched QI during the experiment under pure tension. This behavior also required further investigation, as it may lead to more discovery of DFC's potentials.

As for the numerical modeling aspect, QI is modeled using explicit solver with Hashin's failure criterion. From that, the QI model is used as a template to implement DFC model from Ko *et al.*. According to the result, it can be concluded that Hashin model is not suitable for modeling the non-linear responses happen due to shear load for both QI and

DFC. However, the DFC model is able to capture the strength precisely on all loading configurations. This means the model is able to capture the correct failure mechanisms of DFC. This also serves as an opportunity to examine the fracture energies of DFC model from Ko *et al.*. Furthermore, it is the first time that this model from Ko *et al.* is used under multi-axial configurations, thus validates its capability for those conditions. Finally, from the calibrations, it is found that the fracture energy of DFC exceeds QI by a large amount in mode 2 and 3.

A lot of information and knowledge about QI and DFC has been uncovered in this study, in both experimentally and modeling. However, all of those experimental and modeling results regarding DFCs obtained from this study will only hold valid for the specific specimen size and testing configuration that were conducted. While there are more things to be investigates in this topic, this study would serve as a source for any related researches in the future.

BIBLIOGRAPHY

[1] Carbon Fiber Reinforced Thermoplastic for automobiles. https://www.teijin.com/rd/technology/cfrp/.

[2] Composite World. https://www.compositesworld.com/.

[3] Dassault Systemes ABAQUS. 'ABAQUS Documentation'.

[4] Type of Carbon Fiber Products and their Special Features. https://www.carbonfiber.gr.jp/english/material/type.html.

[5] Understanding CFRP composites. https://www.thoughtco.com/understanding-cfrp-composites-820393.

[6] A. Voloshin and M. Arcan. Pure shear moduli of unidirectional fibre-reinforced materials (FRM). *Fibre Science and Technology*, 1980.

[7] B. Landry and P. Hubert. Experimental study of defect formation during processing of randomly-oriented strand carbon/PEEK composites. *Composites Part A: Applied Science and Manufacturing*, 2015.

[8] B. R. Denos, D. E. Sommer, A. J. Favaloro, R. B. Pipes, and W. B. Avery. Fiber orientation measurement from mesoscale CT scans of prepreg platelet molded composites. *Composites Part A: Applied Science and Manufacturing*, 2018.

[9] Z. P. Bažant. Size effect in blunt fracture: Concrete, rock, metal. *Journal of Engineering Mechanics*, 1984.

[10] B. Boursier. New possibilities with HexMC, a high performance moulding compound. 2001.

[11] C. Qian, L. T. Harper, T. A. Turner, and N. A. Warrior. Notched behaviour of discontinuous carbon fibre composites: Comparison with quasi-isotropic non-crimp fabric. *Composites Part A: Applied Science and Manufacturing*, 2010.

[12] Toray Composites. 2510 prepreg system. 2017.

[13] G. Artner, C. Gerald, P. K. Gentner, J. Nicolics, and C. F. Mecklenbräuker. Carbon fiber reinforced polymer with shredded fibers: Quasi-isotropic material properties and antenna performance. *International Journal of Antennas and Propagation*, 2017.

[14] G. M. Pearce, C. Tao, Y. H. E. Quek, N. T. Chowdhury. A modified Arcan test for mixed-mode loading of bolted joints in composite structures. *Composite Structures*, 2018.

[15] H. Tang, Z. Chen, O. Avinesh, H. Guo, Z. Meng, C. Engler-Pinto, H. Kang, and X. Su. Notch insensitivity in fatigue failure of chopped carbon fiber chip-reinforced composites using experimental and computational analysis. *Composite Structures*, 2020.

[16] Kaj Hollmann. In-plane shear failure analysis of notched composites. *Composites Science and Technology*, 1991.

[17] J. L. Y. Tan, V. S. Deshpande, N. A. Fleck. Failure mechanisms of a notched CFRP laminate under multi-axial loading. *Composites: Part A*, 2015.

[18] J. L. Y. Tan, V. S. Deshpande, N. A. Fleck. Prediction of failure in notched carbon-fibre-reinforced polymer laminates under multi-axial loading. *The Royal Society*, 2016.

[19] J. L. Y. Tan, V. S. Deshpande, N. A. Fleck. The effect of laminate lay-up on the multi-axial notched strength of CFRP panels: Simulation versus experiment. *European Journal of Mechanics A/Solids*, 2017.

[20] J. R. M. d'Almeida, S. N. Monteiro. The iosipescu test method as a method to evaluate the tensile strength of brittle materials. *Polymer Testing*, 1999.

[21] J.M. Finley, M.S.P. Shaffer, S. Pimenta. Data-driven intelligent optimisation of discontinuous composites. *Composite Structures*, 2020.

[22] J.Y. Cognard, L. Sohier, P. Davies. A modified Arcan test to analyze the behavior of composites and their assemblies under out-of-plane loadings. *Composites: Part A*, 2011.

[23] K. Johanson, L. T. Harper, M. S. Johnson, and N. A. Warrior. Heterogeneity of discontinuous carbon fibre composites: Damage initiation captured by digital image correlation. *Composites Part A: Applied Science and Manufacturing*, 2014.

[24] K. Kirane, M. Salviato, and Z.P. Bažant. Microplane-triad model for elastic and fracturing behavior of woven composites. *Journal of Applied Mechanics*, 83(4), 2016.

[25] K. Kirane, M. Salviato, and Z.P. Bažant. Microplane triad model for simple and accurate prediction of orthotropic elastic constants of woven fabric composites. *Journal of Composite Materials*, 50(9):1247–1260, 2016.

[26] S. Ko, K. Chan, R. Hawkins, R. Jayaram, C. Lynch, R. El Mamoune, M. Nguyen, N. Pekhotin, N. Stokes, D. Wu, et al. Experimental and numerical characterization of the intra-laminar fracturing behavior in discontinuous fiber composite structures. In *Proceedings of the 33th ASC Conference, Seattle, WA, USA*, pages 24–26, 2018.

[27] Y. Kumagai, S. Onodera, M. Salviato, and T. Okabe. Multiscale analysis and experimental validation of crack initiation in quasi-isotropic laminates. *International Journal of Solids and Structures*, 193:172–191, 2020.

[28] L. Alfonso, A. Uguen, C. Badulescu, J.-Y. Cognard, T. Bonnemains, E. Lolive, N. Carrere. Determination of the 3D failure envelope of a composite based on a modified Arcan test device. *Composite Structures*, 2015.

[29] M. Alves, D. Carlstedt, F. Ohlsson, L. E. Asp, and S. Pimenta. Ultra-strong and stiff randomly-oriented discontinuous composites: Closing the gap to quasi-isotropic continuous-fibre laminates. *Composites Part A: Applied Science and Manufacturing*, 2020.

[30] M. L. Longana, H. N. Yu, M. Jalavand, M. R. Wisnom, and K. D. Potter. Aligned discontinuous intermingled reclaimed/virgin carbon fibre composites for high performance and pseudo-ductile behaviour in interlaminated carbon-glass hybrids. *Composites Science and Technology*, 2017.

[31] M. Salviato, K. Kirane, S. E. Ashari, Z. P. Bažant, and G. Cusatis. Experimental and numerical investigation of intra-laminar energy dissipation and size effect in two-dimensional textile composites. *Composites Science and Technology*, 2016.

[32] M. Selezneva, S. Roy, L. Lessard, and A. Yousefpour. Analytical model for prediction of strength and fracture paths characteristic to randomly oriented strand (ROS) composites. *Composites Part B: Engineering*, 2016.

[33] M.C. Serna Moreno, J.L. Martínez Vicente, J.J. López Cela. Failure strain and stress fields of a chopped glass-reinforced polyester under biaxial loading. *Composite Structures*, 2013.

[34] N. Eguemann, L. Giger, M. Roux, C. Dransfeld, F. Thiebaud, D. Perreux. Compression moulding of complex parts for the aerospace with discontinuous novel and recycled thermoplastic composite materials. 2014.

[35] P. Feraboli, E. Peitso, T. Cleveland, P. Stickler, J. Halpin. Notched behavior of prepreg-based discontinuous carbon fiber/epoxy systems. *Composites Part A*, 2009.

[36] P. Feraboli, T. Cleveland, M. Ciccu, P. Stickler, and L. DeOto. Defect and damage analysis of advanced discontinuous carbon/epoxy composite materials. *Composites Part A: Applied Science and Manufacturing*, 2010.

[37] P. Feraboli, T. Cleveland, P. Stickler, and J. Halpin. Stochastic laminate analogy for simulating the variability in modulus of discontinuous composite materials. *Composites Part A: Applied Science and Manufacturing*, 2010.

[38] P. Hao, I. Ud Din, S. Panier. Development of modified arcan fixture for biaxial loading response of fiber-reinforced composites. *Polymer Testing*, 2019.

[39] Y. Qiao, A.A. Deleo, and M. Salviato. A study on the multi-axial fatigue failure behavior of notched composite laminates. *Composites Part A: Applied Science and Manufacturing*, 127:105640, 2019.

[40] Y. Qiao and M. Salviato. Micro-computed tomography analysis of damage in notched composite laminates under multi-axial fatigue. *Composites Part B: Engineering*, 187:107789, 2020.

[41] S. Ko, J. Davey, S. Douglass, J. Yang, M. E. Tuttle, M. Salviato. Effect of the thickness on the fracturing behavior of discontinuous fiber composite structures. *Composites Part A*, 2019.

[42] S. Ko, J. Yang, M. E. Tuttle, M. Salviato. Effect of the platelet size on the fracturing behavior and size effect of discontinuous fiber composite structures. *Composite Structures*, 2019.

[43] S. Y. Fu and B. Lauke. The elastic modulus of misaligned short-fiber-reinforced polymers. *Composites Science and Technology*, 1998.

[44] M. Salviato, S.E. Ashari, and G. Cusatis. Spectral stiffness microplane model for damage and fracture of textile composites. *Composite Structures*, 137:170–184, 2016.

[45] M. Salviato, V.T. Chau, W. Li, Z.P. Bažant, and G. Cusatis. Direct testing of gradual postpeak softening of fracture specimens of fiber composites stabilized by enhanced grip stiffness and mass. *Journal of Applied Mechanics*, 83(11), 2016.

[46] M. Salviato, K. Kirane, Z.P. Bažant, and G. Cusatis. Mode I and II interlaminar fracture in laminated composites: a size effect study. *Journal of Applied Mechanics*, 86(9), 2019.

[47] T. Laux, K. W. Gan, J. M. Dulieu-Barton, O. T. Thomsen. A simple nonlinear constitutive model based on non-associative plasticity for UD composites: Development and calibration using a modified Arcan fixture. *International Journal of Solids and Structures*, 2019.

[48] Y. Li, S. Pimenta, J. Singgih, S. Nothdurfter, and K. Schuffenhauer. Experimental investigation of randomly-oriented tow-based discontinuous composites and their equivalent laminates. *Composites Part A: Applied Science and Manufacturing*, 2017.

[49] Y. Wan and J. Takahashi. Tensile and compressive properties of chopped carbon fiber tapes reinforced thermoplastics with different fiber lengths and molding pressures. *Composites Part A: Applied Science and Manufacturing*, 2016.

[50] Y. Wan, I. Straumit, J. Takahashi, and S. V. Lomov. Micro-CT analysis of internal geometry of chopped carbon fiber tapes reinforced thermoplastics. *Composites Part A: Applied Science and Manufacturing*, 2016.

[51] Y. Wan, I. Straumit, J. Takahashi, and S. V. Lomov. Micro-CT analysis of the orientation unevenness in randomly chopped strand composites in relation to the strand length. *Composite Structures*, 2018.

[52] Z. Hashin. Failure criteria for unidirectional fiber composites. *J. Appl. Mech.*, 1980.

[53] Z. P. Bažant, I. M. Daniel, and Z. Li. Size effect and fracture characteristics of composite laminates. *Journal of Engineering Materials and Technology*, 1996.

[54] Z. Rao, L. Ou, Y. Wang, P. Wang. A self-piercing-through riveting method for joining of discontinuous carbon fiber reinforced nylon 6 composite. *Composite Structures*, 2020.